# Characterization of the single *FERONIA* homolog in *Marchantia polymorpha* reveals an ancestral role of *Cr*RLK1L receptor kinases in regulating cell expansion and morphological integrity

Martin A. Mecchia[1#], Moritz Rövekamp[1#+], Alejandro Giraldo-Fonseca[1], Dario Meier[1], Philippe Gadient[1], John L. Bowman[2], and Ueli Grossniklaus[1*]

[1]Department of Plant and Microbial Biology and Zurich-Basel Plant Science Center, University of Zurich, 8008 Zurich, Switzerland

[2]School of Biological Sciences, Monash University, Clayton, Melbourne, Victoria 3800, Australia

[+] Current Affiliation: Department of Aquatic Ecology, EAWAG, 8600 Duebendorf, Switzerland

# These authors contributed equally to the manuscript.

*Author for correspondence: grossnik@botinst.uzh.ch

**Short tittle: Deciphering the ancestral role of *Cr*RLK1L receptors in land plants**

## Summary

Plant cells are surrounded by a cell wall, a rigid structure rich in polysaccharides and glycoproteins. The cell wall is not only important for cell and organ shape, but crucial for intercellular communication, plant-microbe interactions, and as a barrier to the environment. In the flowering plant *Arabidopsis thaliana*, the 17 members of the *Catharanthus roseus* RLK1-like (*Cr*RLK1L) receptor kinase subfamily are involved in a multitude of physiological and developmental processes involving the cell wall, including reproduction, hormone signaling, cell expansion, innate immunity, and various stress responses. Due to genetic redundancy and the fact that individual *Cr*RLK1Ls can have distinct and sometimes opposing functions, it is difficult to assess the primary or ancestral function of *Cr*RLK1Ls. To reduce genetic complexity, we characterized the single *Cr*RLK1L gene of *Marchantia polymorpha*, Mp*FERONIA* (Mp*FER*). Plants with reduced Mp*FER* levels show defects in vegetative development, i.e., rhizoid formation and cell expansion, but also affect male fertility. In contrast, Mp*fer* null mutants and overexpression lines severely affect cell integrity and morphogenesis of the gametophyte. Thus, the *Cr*RLK1L gene family originated from a single gene with an ancestral function in cell expansion and the maintenance of cellular integrity. During land plant evolution, this ancestral gene diversified and was recruited to fulfil a multitude of specialized physiological and developmental and roles in the formation of both gametophytic and sporophytic structures essential to the life cycle of flowering plants.

## Key Words

cell wall integrity, cell elongation, *Cr*RLK1L receptor kinases, *Marchantia polymorpha*, signaling pathway evolution

## Introduction

The functioning of plant cells is contingent upon the cell wall acting as a barrier between the cell and its environment. This complex matrix of polysaccharides, glycoproteins, and other organic compounds defines the growth and shape of a cell and provides protection against biotic and abiotic stresses [1,2]. Moreover, its stiffness has to resist turgor pressure while also allowing cell expansion during growth. Thus, sensing and controlling cell wall integrity (CWI) is crucial for plant cells and receptor kinases (RKs) play an important role in sensing extracellular cues that activate intracellular pathways. Different RK subfamilies are defined by their extracellular domain (ECD), which is more variable than their transmembrane and kinase domains [3]. Over the last decade, the *Cr*RLK1L subfamily emerged as important CWI sensors [4,5].

Functions have been assigned to 15 of the 17 *Cr*RLK1L members encoded in the *A. thaliana* genome: they are required for cell elongation and cell shape, sensing environmental cues, and cell-cell communication in diverse contexts [6–22]. For instance, *FERONIA* (At*FER*), *THESEUS1* (At*THE1*), *HERCULES1* (At*HERK1*), and At*HERK2* are required for cell elongation as At*fer* single, At*the1*At*herk1* double, and At*the1*At*herk1*At*herk2* triple mutants exhibit stunted growth [7,9–11]. Root hairs burst in mutants affecting At*FER* and *[Ca$^{2+}$]$_{cyt}$-ASSOCIATED PROTEIN KINASE1* (At*CAP1*)/*ERULUS* (At*ERU*) [12,16]. Moreover, At*FER* plays a role in powdery mildew resistance [11], innate immunity [15,22], calcium signaling [23], phytohormone signaling [10,24–26], and mechano- and heavy metal sensing [20,27]. In most contexts, the *Cr*RLK1Ls tend to promote cellular growth and cell elongation. In contrast, At*THE1* actively inhibits cell elongation in hypocotyls when cell wall perturbations occur, *e.g.*, due to mutations in the cell wall biosynthesis machinery or upon treatment with isoxaben, a cellulose synthesis inhibitor [7,28].

75 In addition to regulating cellular growth during the vegetative phase of the life cycle,
76 several *Cr*RLK1Ls play a role during fertilization by controlling the growth and reception
77 of the pollen tube. In the female gametophyte, At*FER* is highly expressed in the two
78 synergid cells that flank the egg cell and are important for double fertilization [6,29].
79 At*FER* is crucial for pollen tube reception and the release of the two sperm cells
80 [6,10,23,30,31], a process also involving two other, redundantly acting synergid-
81 expressed *Cr*RLK1Ls, *AtHERK1* and *ANJEA* (*AtANJ*) [17]. In contrast to these synergid-
82 expressed *Cr*RLK1Ls, four pollen-expressed *Cr*RLK1Ls, named *ANXUR1* (At*ANX1*),
83 At*ANX2, BUDDHA'S PAPER SEAL1* (At*BUPS1*) and At*BUPS2* [8,14,18,32], are
84 redundantly required for pollen tube integrity and tip growth.
85 To transduce extracellular cues, *Cr*RLK1Ls bind secreted peptides of the RAPID
86 ALKALINIZATION FACTOR (RALF) family [22,32–35], which induce complex formation
87 with members of LORELEI (LRE) family of GPI-anchored proteins [32,35–37]. Hence, it
88 was suggested that at least some *Cr*RLK1Ls act as CWI sensors that coordinate cell
89 elongation in response to changes in the cell wall [38–43].
90 The 17 *A. thaliana Cr*RLK1Ls act partially redundantly and can have opposite effects on
91 cellular growth (reviewed in [19,41,43,44]). To investigate the original function of
92 *Cr*RLK1Ls, we characterized them in a system with reduced genetic complexity: the
93 liverwort *Marchantia polymorpha* encodes a single *Cr*RLK1L [45,46]. Liverworts represent
94 an early diverging land plant lineage and have been hypothesized to retain, at least in
95 part, characteristics of the earliest land plants [45,47–52]. The presence of similar types
96 of gene families in all plant lineages suggests that the differences in development evolved
97 by co-opting and modifying existing developmental programs and genetic networks,
98 rather than through the evolution of novel genes [47,48,53]. *M. polymorpha* is thus an

99 ideal system to study the ancestral role of genes and how it was modulated and diversified
100 during land plant evolution [45,54,55].
101 We refer to the a single *Cr*RLK1L family member encoded in the *M. polymorpha* genome,
102 Mp4g15890 (Mapoly0869s0001), as Mp*FERONIA* (Mp*FER*) (aka Mp*THESEUS,* Mp*THE*)
103 [44–46,56]. An Mp*fer/the* mutant was identified in a large T-DNA screen for defective
104 rhizoid formation, developing short and irregularly shaped rhizoids with brown tips,
105 indicating rhizoid rupture [56]. In the same screen, a mutant affecting the ortholog of the
106 *A. thaliana* receptor-like cytoplasmic kinase *MARIS* (At*MRI*), known to act downstream of
107 At*FER*, was identified with a similar phenotype (named Mp*mri* aka Mp*pti*, Mp7g17560
108 [Mapoly0051s0094]) [56,57]. As in *A. thaliana*, a dominant active version of Mp*MRI* can
109 partially rescue the Mp*fer* rhizoid phenotype [57]. This suggests that at least some of the
110 machinery associated with cell elongation and CWI sensing is conserved between *A.*
111 *thaliana* and *M. polymorpha*.
112 Here, we report that *Cr*RLK1L function is required in a variety of aspects of *M. polymorpha*
113 gametophyte development. Phylogenetic analyses suggest that *Cr*RLK1L genes first
114 appeared in the common ancestor of land plants. The characterization of lines with
115 reduced Mp*FER* levels indicates that, in addition to its function in rhizoid formation,
116 Mp*FER* controls cell size and organ growth and is involved in male gametogenesis and
117 fertility. Analysis of the Mp*FER* expression pattern points to an involvement in female
118 sexual organogenesis and sporophyte development. Our data suggests that the broad
119 involvement of *Cr*RLK1L function in the development and physiology of land plants is an
120 ancestral and conserved characteristic, although the functions of *Cr*RLK1Ls were
121 extended and adapted to control additional developmental processes in the sporophyte
122 in the course of land plant evolution.
123

124 ## Results

125 ### *Cr*RLK1L is conserved in land plants and arose in this lineage

126 The *M. polymorpha* genome encodes a single *Cr*RLK1L homolog (Mp4g15890
127 [Mapoly0869s0001]) [44–46]. Like other *Cr*RLK1L members, this gene encodes an
128 intracellular serine/threonine kinase domain, a transmembrane domain, and an
129 extracellular malectin-like domain with two malectin domains (Figure 1A). Given that the
130 ECD of *Cr*RLK1Ls in *A. thaliana* is crucial for their function and, in contrast to the kinase
131 domain, not interchangeable [58], we performed a phylogenetic analysis with the amino
132 acid sequences of the predicted malectin-like domain of Mp4g15890, the five members
133 of the moss *Physcomitrella patens*, the two of the lycophyte *Selaginella moellendorffii*,
134 and the 17 *Cr*RLK1Ls of *A. thaliana* (Figure 1B). The *M. polymorpha Cr*RLK1L member
135 grouped together with the *Cr*RLK1Ls of basal land plants and was in the same clade as
136 AtFER, while AtTHE1 was in a different one (Figure 1B). Based on this phylogenetic
137 position and the fact that the malectin-like domain of the *M. polymorpha Cr*RLK1L shared
138 the highest amino acid identity with AtFER (Figure S1A), we named it MpFER [45,46,57],
139 but it is also known as MpTHE [56].

140 Interestingly, no significant similarity to the MpFER malectin-like domain was found when
141 compared to available genomic data of six Chlorophyte algae (*Chlamydomonas*
142 *reinhardtii, Dunaliella salina, Volvox carteri, Coccomyxa subellipsoidea, Micromonas*
143 *pusilla*, *Ostreococcus lucimarinus*) and expression data of six Charophycean algae
144 (*Klebsormidium nitens, Nitella mirabilis, Coleochaete orbicularis, Spirogyra pratensis,*
145 *Mesostigma viride*, *Closterium peracerosum–strigosum–littorale* complex). In *Closterium*
146 complex, an RK named CpRLK1 expressed during sexual reproduction was suggested
147 to be a *Cr*RLK1L homolog [59]. However, comparing the full sequence or the ECD of
148 CpRLK1 with the predicted *M. polymorpha* proteome, higher identity to another RK was

149 found (Figures S1B and S1C). Moreover, no RALF orthologs have been reported in algae,
150 suggesting the origin of the *Cr*RLK1L pathway in land plants [45].
151 To further support MpFER as a member of the *Cr*RLK1L subfamily, the three-dimensional
152 structure of its ECD was modelled [60] using the structure of the AtFER ECD (PDB
153 6a5b.1A, [35]) as a template (Figure 1C). Overall, the predicted structure of the MpFER
154 ECD is highly similar to that of AtFER, keeping an almost identical number of secondary
155 structures (7 alpha-helices and 33 beta-sheets in the MpFER ECD [35] and 8 alpha-helix
156 and 34 beta-sheets in the AtFER ECD, respectively), and a similar spatial disposition for
157 32 of the beta-sheet structures and 6 of the alpha-helices (Figure 1C). When comparing
158 the structural superposition of the AtFER and MpFER ECDs (Figures 1D and S1D), we
159 observed that most conserved parts of the malectin-like domain are in the core of the
160 protein, while the more variable parts are located peripherally. Moreover, the 3D structure
161 of the CpRLK1 ECD could not be properly modelled using the AtFER ECD (Figures S1D
162 and S1E). Taken together, these results suggest that the malectin-like domain of MpFER
163 could interact with similar proteins as AtFER does in *A. thaliana*, and may thus be involved
164 in similar pathways. Sequence comparison of the MpFER kinase domain showed a
165 conservation of the activation loop and a Lys important for catalytic activity (Figure 1E).
166 Furthermore, several determined phosphorylation sites found in AtFER, AtERU, and
167 CrRLK1 were conserved in MpFER (Figure 1E) [13,33,61,62]. Thus, we propose MpFER
168 to be basal and orthologous to all other land plant *Cr*RLK1Ls, and that the *Cr*RLK1L family
169 arose as plants conquered land.
170

171 **Mp*FER* is broadly expressed throughout the *M. polymorpha* life cycle**

172 In *A. thaliana*, the expression patterns of the 17 *Cr*RLK1L members span vegetative and
173 reproductive stages and both generations of the life cycle (reviewed in [43]), pointing to

174 the importance of *Cr*RLK1Ls for basic cellular functions. To assess whether this pattern
175 is reflected in the land plant with the most ancestral characteristics, a promoter fragment
176 of 3.2 kb ($_{pro}$Mp*FER*) was used to drive expression of a triple yellow fluorescent protein
177 (trpVNS) with a nuclear localization signal ($_{pro}$Mp*FER*:*trpVNS*) and transformed into *M.*
178 *polymorpha* sporelings. All transformants expressing the trpVNS fluorescent protein (45
179 of 48 independent lines) exhibited an indistinguishable expression pattern (Figure 2).
180 During vegetative stages of gametophyte development, expression was observed in most
181 cells of the thallus (Figure 2A). In concordance with the importance of Mp*FER* for rhizoids
182 [56], high trpVNS expression was observed in these tip-growing cells (Figure 2B). While
183 trpVNS was expressed in gemma cups, no expression was observed in mature gemmae,
184 possibly due to their dormancy (Figure 2C).
185 In mature female sexual organs, strong expression was observed in the entire
186 archegoniophore (Figure 2D). The archegonia expressed trpVNS in most cells, except for
187 the egg cell (Figure 2E). However, after fertilization, $_{pro}$Mp*FER*:*trpVNS* became active in
188 the zygote (Figure 2F). Inside the sporogonium, the sporogenous cells and subsequently
189 the developing spores, but not the elater cells, strongly expressed trpVNS (Figure 2I). In
190 male sexual organs, trpVNS was broadly detected in the antheridial splash platform
191 (Figure 2G) and, specifically, in the spermatogenous tissue of the antheridia and the non-
192 reproductive jacket cells surrounding them at different developmental stages (Figure 2H).
193 Taken together, Mp*FER* is expressed in most tissues during vegetative stages of
194 gametophyte development as well as in the antheridia and archegonia during the sexual
195 reproduction. Interestingly, the $_{pro}$Mp*FER* promoter is not active in mature gemmae and
196 the unfertilized, quiescent egg cell, although expression is initiated after dormancy and in
197 the zygote. In concordance with the collectively ubiquitous expression of *Cr*RLK1Ls in *A.*

198 *thaliana*, the Mp*FER* expression pattern reinforces the importance of this family for basic
199 cellular functions in land plants.
200
201 **Mp*FER* controls cell expansion during vegetative gametophyte development**
202 To analyze the function of Mp*FER*, three independent artificial microRNA constructs
203 targeting Mp*FER* were designed (amiR-Mp*FER*), based on the endogenous microRNA
204 Mp*miR160* (Figure S2, [63]) and driven by the ubiquitous $_{pro}$Mp*EF1* promoter [64]. While
205 amiR-Mp*FER*1 and amiR-Mp*FER*2 target sites in the ECD coding sequence, amiR-
206 Mp*FER*3 targets the sequence encoding the kinase domain (Figures 3A and 3B). For
207 each amiR-Mp*FER* construct, several independent transgenic lines were obtained that
208 showed a reduction in thallus size (Figures 3C, 3D and S3A). Mp*FER* levels were
209 quantified by qRT-PCR in two independent amiR-Mp*FER*2 and amiR-Mp*FER*3 lines
210 each, which showed a similar phenotype (Figure 3E). Mp*FER* expression ranged from
211 10% to 20% of the wild-type level in all amiR-Mp*FER* lines analyzed (Figure 3E).
212 Previously, the T-DNA insertion mutant Mp*fer-1* was identified in a screen for mutants
213 with defective rhizoids ([56], referred to as Mp*the*). As the T-DNA inserted into the 3' UTR
214 of the Mp*FER* gene (Figure 3A; [56]), Mp*FER* expression was analyzed by qRT-PCR but
215 it showed no reduction compared to the wild type (Figure 3F), suggesting that the T-DNA
216 insertion does not affect Mp*FER* transcription. However, thallus size of Mp*fer-1* mutants
217 is similar to that of amiR-Mp*FER* lines (Figures 3C and 3D), suggesting that MpFER
218 function is partially affected by the T-DNA insertion.
219 Rhizoids are tip-growing cells analogous to the root hairs in flowering plants
220 (angiosperms). Reduced Mp*FER* activity strongly impaired rhizoid formation and the
221 rhizoids collapsed (Figure 3C). This had also been reported for the Mp*fer-1* mutant [56]
222 and is in concordance with the function of At*FER* and At*ANX1/2* in tip-growing root hairs

223 [12,16,33,65] and pollen tubes [8,14], respectively. As *Cr*RLK1L members are important
224 for cell expansion in angiosperms [7,9,11,19,34,66,67], cell size of epidermal thallus cells
225 in fully differentiated regions with minimal growth was measured in Mp*fer-1* and amiR-
226 Mp*FER* lines, showing a reduction in cell area as compared to the wild type (Figures 3G,
227 S3B and S3C). Although amiR-Mp*FER* lines produced more intact rhizoids than Mp*fer-1*
228 mutants (Figure 3C), the average epidermal cell area was similarly reduced, although the
229 distribution of cell areas differed between amiR-Mp*FER* lines and Mp*fer-1* (Figures 3G,
230 S3B and S3C).
231 In conclusion, Mp*FER* has a fundamental role in rhizoid formation and growth during
232 vegetative development. These results suggest an ancestral and conserved function of
233 the *Cr*RLK1Ls in polar cell growth and cell expansion.
234

235 **Mp*FER* is important for the morphological integrity of the gametophyte**

236 Given that Mp*fer-1* and amiR-Mp*FER* lines retain some MpFER activity, we generated
237 Mp*fer* knock-out mutants with the goal to unveil potentially hidden *Cr*RLK1L functions by
238 generating a plant without any *Cr*RLK1L activity. Using CRISPR/Cas9, two sites in the
239 ECD-coding sequence of Mp*FER* were targeted (Figure 4A). At least 10 independent
240 lines were selected and analyzed for each target site. All plants with severely affected
241 thallus development contained a frame shift mutation at the respective target site (Figures
242 4A-4C) while Mp*FER* was not affected in transgenic plants with normal development.
243 The thallus area of the newly generated, amorphic knock-out mutants was more strongly
244 reduced compared to Mp*fer-1* [56], confirming that, like the amiR-Mp*FER* lines, Mp*fer-1*
245 is a hypomorphic mutant (Figures 4C and 4D). In contrast, rhizoid integrity was similarly
246 affected in hypo- and amorphic Mp*fer* alleles, suggesting that rhizoid formation is more
247 sensitive to reduced Mp*FER* activity than thallus growth (Figures 4E-4F). Despite of the

248 strong impact on thallus development, both hypo- and amorphic Mp*fer* mutants form
249 gemma cups.
250 The strong disruption of thallus growth in amorphic Mp*fer* mutants prompted us to
251 investigate whether cells of the thallus died in the absence of Mp*FER* activity. Indeed,
252 using tryphan blue staining, we detected dead cells in these mutants, indicating a loss of
253 morphological integrity (Figure 4G).
254

255 **Some reproductive but not all CWI sensing functions of *Cr*RLK1Ls are conserved**
256 **in land plants**

257 In *A. thaliana*, at least seven *Cr*RLK1L family members play a role in reproduction, with
258 At*ANX1/2* and At*BUPS1/2* being important for pollen tube growth [8,14,18,32] and
259 At*FER*, At*HERK1*, and At*ANJ* for pollen tube reception by the synergid cells [6,17]. To
260 characterize the function of Mp*FER* in reproductive development, amiR-Mp*FER*3-2 lines
261 were transferred to sexual organ-inducing conditions [68]. The number of
262 antheridiophores produced was significantly less in amiR-Mp*FER* lines compared to the
263 wild type (Figures 5A and S3D) and the antheridiophore splash platforms were also
264 smaller (Figure 5B). The reduction in Mp*FER* expression in antheridiophores of amiR-
265 Mp*FER* lines was confirmed by qRT-PCR and results were comparable to those using
266 thallus tissue (Figure 5C). A pronounced reduction in spermatogenous tissue was
267 observed in many antheridia isolated from amiR-Mp*FER*3-2 lines (Figures 5D and 5E).
268 However, although the plants were grown under optimal conditions in axenic culture
269 boxes, the effects on reproductive structures could be partly indirect due to the reduction
270 in plant size and/or rhizoid function.
271 To determine male fertility of these amiR-Mp*FER* lines with reduced spermatogenous
272 tissue, we performed crosses with wild-type female plants. The spermatocyte

273 concentration harvested from wild-type antheridia was almost 3-fold higher than from
274 amiR-Mp*FER* lines and was adjusted using a hemocytometer. In just one of the crosses
275 (n=20), a single sporophyte was formed, resulting in 0.05 ± 0.05 (mean ± SE) sporophytes
276 per archegoniophore, whereas the same females crossed with wild-type males yielded
277 9.95 ± 2.33 (mean ± SE) sporophytes per archegoniophore. In summary, Mp*FER* plays
278 a role in antheridiophore development and spermatocytes of plants with reduced Mp*FER*
279 activity are poorly fertile. Thus, *Cr*RLK1Ls have a conserved role in reproduction in
280 addition to their role in cell expansion and integrity during vegetative development.
281 Some *A. thaliana Cr*RLK1Ls are involved in surveying CWI and in inhibiting growth when
282 CWI is impaired. Cell wall defects caused either by mutations affecting cellulose
283 biosynthesis or by treatment with isoxaben, a cellulose synthesis inhibitor, can be
284 suppressed by a mutation in At*THE1* [7,28]. To investigate whether Mp*FER* also acts as
285 CWI sensor, we treated wild-type, Mp*fer*, and amiR-Mp*FER*3-2 gemmae with isoxaben
286 (Figure 5F). As in the wild type, isoxaben affected the development of gemmae with
287 reduced Mp*FER* activity, all growing progressively less with increasing isoxaben
288 concentration (Figure 5F). These results suggest that the function of At*THE1* in
289 repressing cellular growth when CWI is impaired appeared later in the course of land
290 plant evolution or was lost in the *Marchantia* lineage.
291

292 **The *Cr*RLK1L signaling pathway is conserved in land plants**

293 As downregulation of Mp*FER* or At*FER* produce similar phenotypes concerning polarized
294 growth and cell expansion in *M. polymorpha* and *A. thaliana*, respectively, interspecific
295 complementation was attempted. First, the coding sequence of Mp*FER* fused to the
296 Green Fluorescent Protein (GFP) gene under the control of the viral *35S* promoter
297 ($_{pro}$*35S*:Mp*FER-GFP*) was transformed into heterozygous At*fer-2* mutants. Then, GFP

298 expression at the cell periphery and complementation of the bursting root hair and
299 reduced rosette size phenotypes were assessed in transgenic plants (Figure 6A). At*fer-2*
300 homozygotes expressing the MpFER-GFP protein look similar to At*fer-2* mutants,
301 indicating that Mp*FER* does not complement these At*fer-2* loss-of-function phenotypes
302 (Figure 6A). In a complementary experiment, the coding sequence of At*FER* fused to the
303 Citrine gene under the control of the Mp*EF1* promoter ($_{pro}$Mp*EF1:*At*FER-Cit*) was
304 transformed into amiR-Mp*FER*3-2 plants. Ten independent lines with Citrine expression
305 at the cell periphery were phenotypically characterized (Figures 6B and 6C). All had
306 bursting rhizoids and a reduced thallus size, similar to the parental amiR-Mp*FER*3-2 line,
307 suggesting that At*FER* does not rescue the vegetative phenotypes produced by down-
308 regulation of Mp*FER*.
309 In *A. thaliana*, it was shown that AtFER forms a complex with AtRALF peptides and the
310 LRE/LLG co-receptors [35]. As no interspecific complementation was observed, the
311 conservation of binding surfaces between *Cr*RLK1L, RALF, and LRE homologs were
312 analyzed. The *M. polymorpha* genome encodes three RALF peptides (MpRALF:
313 Mp1g27120 [Mapoly0002s0166]; MpRALF2: Mp2g21670 [Mapoly0040s0047];
314 MpRALF3: Mp7g07270 [Mapoly0076s0067]) [44,45]. We performed a phylogenetic
315 analysis using the amino acid sequences of the predicted mature peptides of *A. thaliana*
316 and *M. polymorpha* RALFs (Figure S4A). All MpRALF peptides clustered together with
317 AtRALFs known to interact with *Cr*RLK1L receptors, including AtRALF1 and AtRALF23,
318 which serve as AtFER ligands [22,33] (Figure S4A). The MpRALFs shared the four
319 conserved Cys residues as well as the YXXY and YY motifs with the AtRALF1 subgroup
320 (Figure S4B). However, only MpRALF1 and MpRALF3 had an RRXL motif important for
321 S1P cleavage (Figures S4B and S4C)[69], consistent with the presence of one S1P
322 ortholog in basal plants (Mp8g07990 [Mapoly0155s0018], Figure S4D). There are two

323 MpLRE/LLG proteins encoded in the *M. polymorpha,* genome (Figure S5A). Both the
324 MpLRE1 (Mp5g09600 [Mapoly0048s0110]) and MpLRE2 (Mp4g22100
325 [Mapoly0090s0020]) proteins showed conservation of the eight Cys and the ND motif
326 distinctive of the family (Figure S5B); however, MpLRE1 did not contain a GPI anchoring
327 site (Figure S5B). Structure prediction using AtLLG2 as a template [35] showed a
328 conserved general structure (Figures S5C and S5D). Some of the Mp*RALF* and Mp*LRE*
329 family members show a similar expression pattern as Mp*FER* (Figure S5F), suggesting
330 that the corresponding proteins could form a complex similar to that described in *A.*
331 *thaliana*.
332 To gain insights into the formation of a putative *Cr*RLK1L signaling complex, the
333 MpFER/MpRALF/MpLRE complex was modelled. The general structure appeared
334 conserved (Figure S5E); however, analysis of conserved sites between *M. polymorpha*
335 and *A. thaliana* showed a low amino acid conservation in the interacting surfaces of the
336 complex subunits (Figure 6D). This suggests that the lack of interspecific
337 complementation may be due to differences in amino acids that are important for complex
338 formation, and that the proteins forming the complex have diverged, following distinct
339 routes of co-evolution in the two lineages.
340 Because interspecific complementation of the amiR-Mp*FER* phenotypes was
341 unsuccessful, we asked whether suppression using a downstream component of
342 *Cr*RLK1L signaling identified in *A. thaliana* was possible. AtMRI, a receptor-like
343 cytoplasmic kinase, acts downstream of At*FER* or At*ANX1/2* in the regulation of polar tip
344 growth [70,71]. The dominant AtMRI$^{R240C}$ mutation can suppress pollen tube rupture in
345 the At*anx1*/At*anx2* double mutant and the root hair defects of At*fer-4* [70,71]. A mutation
346 in Mp*MRI* (aka Mp*PTI*) with a similar bursting rhizoid phenotype as observed in Mp*fer-1*,
347 was identified in the same genetic screen for *M. polymorpha* mutants with defective

348 rhizoids [56]. To test whether Mp*MRI* is a conserved downstream component of the
349 Mp*FER* signal transduction pathway, a dominant-active form of the protein equivalent to
350 AtMRI$^{R240C}$ was transformed into the amiR-Mp*FER*3-2 line, driven by 2 kb of the
351 endogenous promoter ($_{pro}$Mp*MRI:*Mp*MRI$^{R240C}$*). Several independent lines showed a
352 partial restoration of rhizoid growth; however, we also observed defects in thallus
353 development of lines with higher levels of Mp*MRI* expression, mainly abnormalities in the
354 epidermis (Figures 6E and S6A-S6E). This suggest that Mp*MRI* acts downstream of
355 Mp*FER* in the signal transduction pathway controlling polarized growth since the origin of
356 land plants, in agreement with a recent report on the functional characterization of Mp*MRI*
357 [57].
358

359 **Overexpression of Mp*FER* affects morphological integrity**

360 Because overexpressing At*FER* in *M. polymorpha* did neither lead to any obvious
361 phenotypes nor complementation of amiR-Mp*FER* lines (Figures 6B and 6C), we also
362 overexpressed At*FER* and Mp*FER* in the wild type. As in the amiR-Mp*FER* background,
363 overexpression of AtFER ($_{pro}$Mp*EF1:*At*FER-Cit*) in a wild-type background had no effect,
364 consistent with the idea that At*FER* is unable to form a complex with the corresponding
365 *M. polymorpha* proteins. However, when expressing an MpFER-Citrine fusion protein
366 ($_{pro}$Mp*EF1:*Mp*FER-Cit*) in wild-type plants, thallus development was strongly affected
367 (Figure 7A). As expected, MpFER-Cit localized to the membrane (Figure 7B), and higher
368 protein levels correlated with more severe phenotype (Figures 7A and 7C). Scanning
369 electron microscopy of epidermis of plant expressing high levels of Mp*FER* showed
370 defects in the formation of air chambers and air pores (Figure 7D), similar to what we
371 observed when expressing the dominant-active Mp*MRI$^{R240C}$* (Figure S6A-S6C).
372 Moreover, overexpression of MpFER affects the number of lobes in the antheridial

373 receptacle, producing only 4 instead of 8 (Figure S6F), supporting the importance of
374 MpFER during sexual development. Considering the importance of Mp*FER* for normal
375 rhizoid formation, we also analyzed rhizoids in the $_{pro}$Mp*EF1:*Mp*FER-Cit* lines: while
376 rhizoid morphology looked normal, a decrease in rhizoid number was observed (Figures
377 7E and 7F).
378 Taken together, the results obtained by overexpressing Mp*FER* support the role of
379 Mp*FER* in cell expansion and maintaining tissue integrity during plant morphogenesis.
380

381 ## Discussion

382 During land plant evolution, many developmental aspects have changed in order to adapt
383 to new environments, producing the enormous diversity observed in the plant kingdom.
384 However, the control and maintenance of CWI remained a key aspect for the biology of
385 a plant cell. CWI sensing is not only important for vegetative growth by cell expansion,
386 but it is also essential for sexual reproduction and defense responses.
387 The *Cr*RLK1L family was first characterized for its importance during angiosperm
388 fertilization, a process comprising aspects of polar cell elongation, CWI control, and cell-
389 cell communication [6,30,31]. Lately, different members of this family were found to carry
390 out diametrically opposite roles in diverse aspects of plant development, which has made
391 it difficult to define the core or ancestral function of this gene family comprising 17-
392 members in *A. thaliana* [6–12,14–20,32].
393 Here, we report the characterization of the single *Cr*RLK1L gene encoded in the genome
394 of *M. polymorpha*. Structurally, the MpFER ECD and kinase domain share similarities
395 with previous characterized *Cr*RLK1L members, including the malectin-like domain and
396 conserved phosphorylation sites. Conservation of RALF and LRE members in *M.*
397 *polymorpha* suggests that MpFER also forms a complex at the plasma membrane [35].

398 While modeling predicted that the general structure of the complex was conserved, the
399 interaction surfaces seem to have diverged and co-evolved independently in the
400 respective lineages.

401 We observed a broad involvement of Mp*FER* at both vegetative and reproductive stages
402 of development: During vegetative growth of the gametophyte, Mp*FER* is required for
403 rhizoid formation and cell expansion but it also plays a role in male gametogenesis and
404 is expressed in female reproductive organs. These findings suggest that the *Cr*RLK1Ls
405 have, also in ancestral land plants, held roles in various aspects of both vegetative and
406 reproductive development. Thus, the role of *Cr*RLK1Ls in angiosperm reproduction does
407 not represent a derived feature from a purely vegetative function in cell elongation in
408 bryophytes, but constitutes a conserved feature of this gene family.

409 Moreover, the almost ubiquitous expression of Mp*FER* in *M. polymorpha* is consistent
410 with the collective expression of different *Cr*RLK1L members in essentially all tissues and
411 organs of *A. thaliana* [43]. Thus, gene duplication allowed the expansion of the *Cr*RLK1L
412 family in angiosperms, diversifying their expression patterns and functions but also
413 leading to genetic redundancy [8,17,32,43].

414 *Cr*RLK1L members are important sensors of CWI during polarized growth, both in pollen
415 tubes [8,32] and root hairs [16]. In early divergent land plants, rhizoids are tip-growing cell
416 with a function analogous to that of root hairs, important for taking up nutrients and water
417 [56,72]. Based on the conservation of many genes controlling the development and
418 growth of tip-growing cells forming rooting systems, it was suggested that these pathways
419 were active in the earliest land plants that existed about 470 million years ago [56]. That
420 Mp*FER* also controls rhizoid integrity points to the importance of the *Cr*RLK1L pathway
421 for polarized growth since the origin of land plants. Moreover, the fact that amorphic Mp*fer*
422 mutants contain many dead cells demonstrates the importance of the *Cr*RLK1L pathway

423 for cellular integrity during vegetative growth. This aspect has not yet been reported for
424 *A. thaliana Cr*RLK1L mutants, possibly due to genetic redundancy among family
425 members.
426 The signaling mechanisms downstream of Mp*FER* in *M. polymorpha* development are
427 still unclear. Mp*MRI*, the *M. polymorpha* ortholog of At*MRI*, which acts downstream of
428 AtFER and AtANX1/2 in *A. thaliana* during polarized growth [70], does have a similar
429 rhizoid phenotype as Mp*FER* [56,57]. The suppression of the rhizoid phenotype in amiR-
430 Mp*FER* transformants with the constitutively active form MpMRI$^{R240C}$ corroborates a
431 conserved *Cr*RLK1L signaling cascade during polarized growth in *M. polymorpha* but
432 whether this pathway also relies on $Ca^{2+}$ and reactive oxygen species (ROS) as second
433 messengers as it does in *A. thaliana* remains to be determined.
434 In *A. thaliana*, loss-of-function mutations in the motor protein AtKINESIN-13a, a
435 microtubule-based motor, cause cell elongation in petals, leaves, and hypocotyls
436 concomitant with changes in cell wall composition in leaves [73]. This effect depends on
437 functional AtTHE1 and does not occur in At*kinesin-13-a/*At*the1* double mutants.
438 Interestingly, in this case, AtTHE1 stimulates cell elongation in response to defects in cell
439 wall deposition [73]. Based on our results, we have no indication that Mp*FER* acts as a
440 CWI sensor and regulates growth similar to At*THE1* in response to cell wall disturbances.
441 We have not observed a context in *M. polymorpha* development in which Mp*FER* inhibits
442 cell expansion. Therefore, the ability to restrict growth in response to disturbances in CWI
443 could represent an evolutionary derived feature, as gene duplication allowed for the
444 diversification and specialization of *Cr*RLK1Ls to regulate cellular growth in a more
445 complex and context-dependent way. The capacity to flexibly regulate growth appears to
446 be fundamentally context-dependent, as a similar discrepancy in promoting or inhibiting
447 growth is also known for some well-studied growth promoting agents, like the

448 phytohormones auxin and brassinosteroid, which can have growth-inhibitory effects
449 dependent on tissue and concentration. The reverse was noted for the phytohormones
450 ethylene and abscisic acid, which are usually considered growth inhibitors but can also
451 promote growth, dependent on the context [74–76].
452 Taken together, our results suggest an ancestral and conserved function of the *Cr*RLK1Ls
453 in polar cell growth and cell expansion, but also during sexual reproduction. In addition,
454 we probe the relevance of *Cr*RLK1L members for cell integrity and morphogenesis. In
455 angiosperms, *Cr*RLK1Ls occupy an important position at the interface of developmental
456 and environmental inputs, which are integrated by a downstream signaling machinery
457 that controls cell shape and polar growth to ensure normal development, *e.g.* by
458 preventing cell rupture upon CWI defects. Whether the same downstream machinery is
459 utilized in a similar fashion in *M. polymorpha* remains to be shown, even though the
460 similarity in function points to a related mechanism. Even less is known about upstream
461 aspects of *Cr*RLK1L signaling. Future studies on the transcriptional regulation and the
462 upstream components, such as the putative RALF ligand(s), in the highly simplified *M.*
463 *polymorpha* system could provide fundamental insights into the molecular mechanism of
464 the *Cr*RLK1L pathway, which is so central to land plant physiology, growth, and
465 development.
466

467 ## Acknowledgments

468 We thank Liam Dolan for kindly providing the Mp*fer-1*/Mp*the* mutant, Valeria Gagliardini
469 for help with qRT-PCR and ddPCR, Anja Grossniklaus for help in measuring epidermal
470 cell area, Célia Baroux and Ethel Mendocillo-Sato for instructions on confocal microscopy
471 and the use of Imaris Software, Isabel Monte and Cyril Zipfel for comments on the

manuscript, and Christof Eichenberger, Frédérique Pasquer, Arturo Bolaños, Daniela Guthörl, Daniel Prata, and Peter Kopf for general lab support.

## Author contributions

MAM: Conceptualization, Formal analysis, Investigation, Methodology, Validation, Visualization, Writing – original draft, Writing – review & editing

MR: Conceptualization, Formal analysis, Investigation, Methodology, Validation, Visualization, Funding acquisition, Writing – original draft, Writing – review & editing

AF-G: Data curation, Formal analysis, Software, Validation, Visualization, Writing – original draft, Writing – review & editing

DM: Formal analysis, Investigation, Validation, Writing – review & editing

PG: Formal analysis, Investigation, Validation, Writing – review & editing

JLB: Funding acquisition, Resources, Supervision, Validation, Writing – review & editing

UG: Conceptualization, Formal analysis, Funding acquisition, Project administration, Supervision, Validation, Writing – original draft, Writing – review & editing

## Funding disclosure

This work was supported by the University of Zurich, Monash University, and grants from the Forschungskredit of the University of Zurich (http://www.research.uzh.ch/en/funding/phd/fkcandoc; FK-16-090) to MR, the Australian Research Council (http://www.arc.gov.au; DP130100177) to JLB, and the Swiss National Science Foundation (http://www.snf.ch; 310030B_160336 and 31003A_179553) to UG. The funders had no role in study design, data collection and analysis, decision to publish, or preparation of the manuscript.

496

## Competing interests

498 The authors have declared that no competing interests exist.

499

## Main figure titles and legends

501 **Figure 1. *Cr*RLK1Ls Are Conserved among Land Plants**

502 (A) Representation of AtFER and MpFER proteins. Malectin-like domains are
503 represented in blue and kinase domains in green. SP, signal peptide; TM, transmembrane
504 domain (yellow). Amino acids important for regulation and activity are marked in red,
505 violet, and light blue as described in Figure 1E.

506 (B) A rooted neighbor-joining tree of the amino acid sequence of the predicted malectin-
507 like domain. *Cr*RLK1L members from *Marchantia polymorpha* (Mp), *Physcomitrella*
508 *patens* (Pp), *Selaginella moellendorffii* (Smo), and *Arabidopsis thaliana* (At) were used.
509 The numbers indicate the bootstrap values (%) from 1000 replications. The given scale
510 represents a substitution frequency of 0.1 amino acids per site.

511 (C) Cartoon representation of the predicted three-dimensional structure of the MpFER
512 malectin-like domain, showing predicted alpha-helix and beta-sheet structures.

513 (D) Structural superposition of the malectin-like domains of AtFER (blue) and MpFER
514 (green).

515 (E) Alignment of the cytoplasmic domains of MpFER, AtERU, AtFER, and *Cr*RLK. Kinase
516 domains are in green, putative phosphorylation sites in light blue (Ser) and violet (Thr),
517 and the conserved catalytic Lys in red.

518 See also Figure S1

519

520 **Figure 2. Mp*FER* Is Broadly Expressed in most Tissues throughout the *M.***
521 ***polymorpha* Life Cycle**

522 Expression of $_{pro}$Mp*FER*:*trpVNS* in different organs of male and female *M. polymorpha*
523 plants. Fluorescence is visualized as either green (epifluorescence microscope) or yellow
524 (confocal microscope) color, depending on the panel.

525 (A to D) Bright field (left) and epifluorescence (right) images of a thallus, (A) rhizoid (C),
526 gemmae cups (C), and an archegoniophore (D). Red arrows indicate meristematic zones,
527 the yellow arrow gemmae. Scale bars, 0.5 mm.

528 (E and F) Confocal images of archegonia before (E) and 2 days after fertilization (F).
529 Scale bar, 50 µm.

530 (G) Bright field (left) and epifluorescence (right) images of an antheridiophore. Scale bar,
531 1 mm.

532 (H) Confocal image of antheridia. Scale bar, 100 µm.

533 (I) Confocal image of sporophyte and spores. Scale bar, 25µm.

534

535 **Figure 3. Mp*FER* Controls Cell Size during Gametophyte Development**

536 (A) Representation of the mature Mp*FER* mRNA. Coding sequence are in green,
537 locations of the amiRNA target sites in blue.

538 (B) Base complementary between mature amiR-Mp*FER*1, amiR-Mp*FER*2, and amiR-
539 Mp*FER*3 with the Mp*FER* transcript.

540 (C) Relative expression level of Mp*FER* in thallus tissue from wild-type (WT; Tak1) and
541 two independent insertion lines of amiR-Mp*FER*2 and amiR-Mp*FER*3, as measured by
542 qRT-PCR. Mp*EF1* was used as internal control. Shown are means ± standard errors of
543 the means (SEM) of three biological replicates. *P < 0.01, one-way analysis of variance
544 (ANOVA).

545 (D) Relative expression level of Mp*FER* in WT and Mp*fer-1* thallus tissue, as measured
546 by qRT-PCR. Mp*EF1* was used as internal control. Shown are means ± SEM of three
547 biological replicates. *P < 0.01, one-way ANOVA.
548 (E) Representative pictures of 10-day old gemmalings of WT, Mp*fer-1*, and amiR-
549 Mp*FER*3-2 lines. Scale bar, 1 mm.
550 (F) Thallus area of WT, Mp*fer-1*, and amiR-Mp*FER*3-2 lines. n = 30, outliers are indicated
551 as black dots.
552 (G) Violin plot of cell size in WT, *Mpfer-1*, and amiR-Mp*FER*3-2 lines. Significant
553 differences are indicated according to the non-parametric Kruskal-Wallis test and linear
554 regression models (***p<0.001).
555 See also Figures S2 and S3
556
557 **Figure 4. The Integrity of Thalli from Mp*fer* Knock-out Lines Is Severely Affected**
558 (A) Representation of the mature Mp*FER* mRNA with the coding sequence in green, and
559 the location of the gRNA target sites in red.
560 (B) Sequences of gRNA target sites in the confirmed Mp*fer* knock-out mutants. Deletions
561 and insertions are highlighted in red.
562 (C) Representative pictures of 10-day old gemmalings of WT, Mp*fer-1*, and two
563 independent Mp*fer* knock-out mutants. Scale bar, 0.5 cm.
564 (D) Thallus area of 10-day old gemmalings of WT, Mp*fer-1*, and two independent Mp*fer*
565 knock-out mutants. n = 30.
566 (E) Representative pictures of 3-day old gemmalings growing in upside-down plates of
567 WT, Mp*fer-1*, and two independent Mp*fer* knock-out mutants. Scale bar, 500 μm.
568 (F) Rhizoid number in 3-day old gemmalings of WT, Mp*fer-1*, and two independent Mp*fer*
569 knock-out mutants. n = 30.

570 (G) Trypan blue staining of 7-days old gemmalings of WT, Mp*fer-1*, and two independent
571 Mp*fer* knock-out mutants. Scale bar, 1 mm.
572
573 **Figure 5. Conservation of *Cr*RLK1L Function in Land Plants**
574 (A) Number of antheridiophores produced per plant for wild-type (WT, n=9) and two
575 independent amiR-Mp*FER*3 lines (amiR-Mp*FER*3-2, n = 9; amiR-Mp*FER*3-3, n = 12).
576 Shown are means ± SEM of two biological replicates. Means with same letter do not differ
577 significant different with P > 0.05, one-way ANOVA, Duncan test.
578 (B) Antheridiophore splash platform size distribution of WT (n = 32), amiR-Mp*FER*2-3 (n
579 = 34), and amiR-Mp*FER*3-3 (n = 11) lines. For all antheridia with a stalk >8 mm, length
580 and width of the platform were recorded.
581 (C) qRT-PCR of Mp*FER* levels in antheridiophores in a WT and amiR-Mp*FER*3-3 line.
582 Mp*EF1* was used as internal control. Shown are means ± SEM of three biological
583 replicates. *P < 0.01, ANOVA.
584 (D and E) Mature antheridia of a WT (D) and amiR-Mp*FER*3-3 line (E). Bright field images
585 (left) and in cross-section (right). The spermatogenous areas are indicated in red. Scale
586 bar, 100*μ*m.
587 (F) Thallus area of 15-day old gemmalings of WT, *Mpfer-1* mutant, and an amiR-
588 Mp*FER*3-2 line growing on media containing different isoxaben concentrations (nM). n =
589 30, outliers are indicated as black dots. Shown are means ± SEM of two biological
590 replicates. Means designated by the same letter do not significantly differ at P > 0.05,
591 one-way ANOVA, Duncan test.
592 See also Figure S3
593

594 **Figure 6. Interspecific Complementation of *A. thaliana* and *M. polymorpha* Plants**
595 **with Reduced Levels of *FER* Activity**

596 (A) Roots of independent *A. thaliana* lines expressing 35S*:*Mp*FER-GFP* in L*er* wild-type
597 (WT) and At*fer-2* plants. Scale bar, 200 µm.

598 (B) 10-day old gemmalings of WT and amiR-Mp*FER*3-2 *M. polymorpha* plants with and
599 without expression of At*FER-Cit*. Scale bar, 0.5 mm.

600 (C) Citrine expression in 7-day old gemmalings of WT and amiR-Mp*FER*3-2 plants with
601 and without expression of At*FER-Cit*. Scale bar, 100 µm.

602 (D) Cartoon representation of the structural conservation of the *Cr*RLK1L$^{ECD}$/LRE/RALF
603 complex by comparing AtFER/MpFER and AtLLG2/MpLRE1. Blue and green represent
604 spatially highly conserved regions of *Cr*RLK1L and LRE homologs, respectively. Red
605 indicates structural regions with low spatial conservation, lilac the C-terminal part of
606 AtRALF23, and black arrows the interaction regions of the three proteins.

607 (E) Complementation of amiR-Mp*FER* lines with a dominant-active version of Mp*MRI*
608 under its own promoter ($_{pro}$Mp*MRI*:*MRI*$^{R240C}$). Scale bar, 1 mm.

609 See also Figures S4-S7

610

611 **Figure 7: Overexpression of Mp*FER* Affects Morphological Integrity**

612 (A) Representative pictures of 10-day old gemmalings of wild-type (WT, Tak1) and
613 different lines overexpressing Mp*FER* ($_{pro}$Mp*EF1:*Mp*FER-Cit)*. Scale bar, 1 mm.

614 (B) Citrine expression at the plasma membrane in WT and $_{pro}$Mp*EF1:*Mp*FER-Cit* lines *#5*
615 and #9 as observed under confocal microscopy. Scale bar, 20 µm.

616 (C) Western blot analysis of $_{pro}$Mp*EF1:*Mp*FER-Cit* lines using an anti-GFP antibody.
617 $_{pro}$Mp*EF1:Cit* and WT lines were used as positive and negative controls, respectively. The

618 Ponceau membrane staining of the most intense band at 55 kDa (presumably Rubisco)
619 was used as a loading control.
620 (D) Scanning electron microscopical images of thalli from 20-day old plants of WT and
621 $_{pro}$Mp*EF1:*Mp*FER-Cit* lines #*5* and #9. Scale bar, 500 µm.
622 (E) Representative pictures of 3-day old gemmalings growing in upside-down plates of
623 WT and $_{pro}$Mp*EF1:*Mp*FER-Cit* lines #*5* and #9. Scale bar, 1 mm.
624 (F) Number of rhizoids in 3-day old gemmalings of WT and $_{pro}$Mp*EF1:*Mp*FER-Cit* lines #*5*
625 and #9. n = 30.
626 See also Figure S6
627

628 ## Supplemental figure titles and legends

629

630 **Figure S1. The *Cr*RLK1L Family Appeared together with Land Plants. Related to**
631 **Figure 1.**
632 (A) Percentage of identity of the malectin-like domain, the complete ECD, and the full
633 protein of MpFER with AtFER, AtANX1, AtANX2, and AtTHE1.
634 (B) Percentage of identity of the ECD and full protein of CpRLK1 with MpFER, AtFER,
635 and Mapoly001s0111.
636 (C) A rooted neighbor-joining tree of the amino acid sequence of the predicted malectin-
637 like domain was generated using ClustalW. *Cr*RLK1L members from *Marchantia*
638 *polymorpha* (Mp), *Physcomitrella patens* (Pp), *Selaginella moellendorffii* (Smoe), and
639 *Arabidopsis thaliana* (At) were used. Algal CpRLK1 and Mapoly001s0111 were also
640 included. The numbers indicate the bootstrap values (%) from 1000 replications. The
641 given scale represents a substitution frequency of 0.1 amino acids per site.

642 (D) Qmean value for prediction of MpFER or CpRLK1 3D structures of the ECD based
643 on the AtFER ECD. Green numbers indicate a good modelling fit, red numbers indicates
644 a bad modelling fit.
645 (E) Structural superposition of the ECD of AtFER (blue) and CpRLK1 (purple).
646
647 **Figure S2. Design of amiR-Mp*FER* Precursors. Related to Figure 3.**
648 (A) Mp*miR160* (Mapoly0002s0211, Mp1g26670) and amiR-Mp*FER*1, amiR-Mp*FER*2,
649 and amiR-Mp*FER* sequences. miRNA sequences are in red and miRNA* in blue. Cloning
650 sequences from amiR-Mp*FER* constructs are in bold.
651 (B) Drawing of the minimum free energy structure of Mp*miR160* and amiR-Mp*FER*3
652 constructs predicted by the RNAfold web server (http://rna.tbi.univie.ac.at//cgi-
653 bin/RNAWebSuite/RNAfold.cgi). Red arrows indicate location and orientation of the
654 mature miRNA in the precursor. The structures are colored by base-pairing probabilities;
655 for unpaired regions the color denotes the probability of being unpaired.
656
657 **Figure S3. Reduction in Thallus and Cell Area in Plants with Reduced Mp*FER***
658 **Levels. Related to Figures 3 and 5.**
659 (A) Thallus area of wild-type (WT), Mp*fer-1*, and amiR-Mp*FER*3-2 plants at different days
660 after putting gemmae on plates. n = 30, outliers are indicated as black dots. Areas were
661 estimated using ImageJ software.
662 (B) Representative images from cell surface areas measured in WT, amiR-Mp*FER*2-1,
663 and amiR-Mp*FER*3-2 plants. Scale bar, 50 *µ*m.
664 (C) Difference in cell size between WT, amiR-Mp*FER*2-1, *and* amiR-Mp*FER*3-2 plants is
665 significant ($p<0.001$) based on the nonparametric Kruskal-Wallis test and a linear
666 regression model with a highly significant interaction ($p<0.001$).

667 (D) Induction of antheridiophores in WT and two independent amiR-Mp*FER*3 lines. Three
668 plants were grown in each sterile plastic box under far-red light induction.
669
670 **Figure S4. MpRALF Peptides Belong to the AtRALF1-clade of the RALF Family.**
671 **Related to Figure 6.**
672 (A) A rooted neighbor-joining tree of the amino acid sequence of the predicted mature
673 RALF peptides was generated using ClustalW. RALF members from *M. polymorpha* and
674 *A. thaliana* were used. Red arrows indicate RALFs that are known ligands of *Cr*RLK1Ls.
675 The numbers indicate the bootstrap values (%) from 1000 replications. The given scale
676 represents a substitution frequency of 0.1 amino acids per site.
677 (B) Amino acid sequence comparison of AtRALF1 and MpRALF1-3. Predicted signal
678 peptides are in black, predicted mature peptides in light blue, conserved Cys in red, and
679 predicted S1P recognition sites in violet.
680 (C) Processing pathway AtRALF1 by the S1P protease.
681 (D) A rooted neighbor-joining tree of the amino acid sequence of the S1P orthologs was
682 generated using ClustalW. S1P members from *M. polymorpha*, *P. patens*, and *A. thaliana*
683 were used. The numbers indicate the bootstrap values (%) from 1000 replications. The
684 given scale represents a substitution frequency of 0.1 amino acids per site.
685
686 **Figure S5. Two LORELEI-like Proteins Are Encoded in the *M. polymorpha* Genome.**
687 **Related to Figure 6.**
688 (A) A rooted neighbor-joining tree of the amino acid sequence of LRE orthologs was
689 generated using ClustalW. LRE members from *M. polymorpha*, *P. patens*, and *A. thaliana*
690 were used. The numbers indicate the bootstrap values (%) from 1000 replications. The
691 given scale represents a substitution frequency of 0.1 amino acids per site.

692 (B) Amino acid sequence of AtLRE, MpLRE1, and MpLRE2. Conserved Cys are in light
693 blue, the ND motif in red, and the GPI-anchoring site in green.
694 (C) Cartoon representation of the predicted 3-dimensional structure of MpLRE1, showing
695 predicted alpha-helices.
696 (D) Structural superposition of AtLGG2 (blue) and MpLRE1 (green).
697 (E) Cartoon representation of the predicted 3-dimensional structure of the
698 MpFER/MpLRE1/MpRALF1 complex, showing predicted alpha-helices and beta-sheets.
699 (F) Heatmap depicting relative gene expression based on RNAseq data (row-Z-score of
700 vs normalized counts) of Mp*FER* and the *M. polymorpha* orthologs of At*MR*I, At*RALF1*,
701 and At*LRE* across different tissues. Vegetative and reproductive tissues are grouped by
702 green and orange, respectively. Averaged expression values are represented with colors
703 of increasing red and blue intensity indicating upregulation and downregulation of gene
704 expression, respectively.
705
706 **Figure S6. Expression of Mp*MRI*$^{R240C}$ Suppresses the Bursted Rhizoid Phenotype**
707 **of amiR-Mp*FER*3 Lines but Leads to Aberrant Epidermis Development. Related to**
708 **Figures 6 and 7.**
709 (A to C) Epidemical pictures of thalli from the wild-type (WT, Tak-1) (A), and amiR-
710 Mp*FER*3 + $_{pro}$MpMRI:Mp*MRI*$^{R240C}$ lines #6 (B) and #8 (C), which both partially suppressed
711 the bursting rhizoid phenotype (Fig. 6).
712 (D and E) Relative expression of Mp*FER* (D) and Mp*MRI* (E) against the geometric mean
713 of the reference genes Mp*ACT1*, Mp*ACT7*, and Mp*APT3* in WT, amiR-Mp*FER*3-2, and 5
714 lines (#5 to #9) co-transformed with the amiR-Mp*FER*3-2 and $_{pro}$MpMRI:Mp*MRI*$^{R240C}$
715 constructs. Expression levels of three biological replicates were assessed by droplet
716 digital PCR (ddPCR). The y-axis corresponds to the log2-ratio between the test and the

717 geometric mean of the reference genes. Shown are means ± SEMs of three biological
718 replicates. *P < 0.01, one-way ANOVA.
719 (F) Representative images of the antheridial receptacle of WT and $_{pro}$Mp*EF1:*Mp*FER-Cit*
720 plants. Scale bar, 2 mm.
721
722 **Figure S7. Structure Assessment and Quality Estimations of the MpFER and**
723 **MpLRE 3-dimensional Models. Related to Figure 6.**
724 QMEAN score barplot indicating quality estimates of the predicted models, across their
725 aminoacidic sequence. Below the barplots, the corresponding secondary structures are
726 displayed for both target and template sequences, with alpha-helixes represented by light
727 purple boxes and beta-sheets by green arrows. All plots were adapted from the model
728 report produced by the SWISS-MODEL workspace.
729 (A) MpFER$^{ECD}$, for which AtFER was used as a template (PDB 6a5b.1A).
730 (B) MpLRE1, for which AtLLG2 was used as a template (PDB 6a5d.1A).
731

732 # RESOURCE AVAILABILITY

733

734 ## Lead Contact

735 Further information and requests for resources and reagents should be directed to and
736 will be fulfilled by the Lead Contact, Ueli Grossniklaus (grossnik@botinst.uzh.ch).
737

738 ## Materials Availability,

739 Requests for other strains and plasmids should be directed to the Lead Contact.
740

741 ## Data and Code Availability.

742 This study did not generate datasets or code.

743

744 ## EXPERIMENTAL MODEL AND SUBJECT DETAILS

745 *M. polymorpha* subsp. ruderalis plants were grown on sterile culture on half-strength
746 Gamborg's B5 basal medium (PhytoTechnology Laboratories), supplemented with 1%
747 phytoagar in Petri dishes sealed with air-permeable tape. The plants were kept under
748 fluorescent light and long-day conditions (16 h light at 22ºC, 8 h dark at 20 ºC) in Percival
749 growth cabinets (models AR-41L3 and AR-41/L2). Alternatively, to induce sexual
750 reproduction, plants were cultivated in jiffy pots filled with a 1:1 mixture of soil
751 ("Einheitserde D73 + Bims", Universalerde) and sand or in culture boxes in sterile culture
752 on half-strength Gamborg's B5 basal medium (Duchefa Eco2 Box, #E1654), under
753 fluorescent light supplemented with far-red light (GreenPower LED module HF far-red,
754 #929000464503 and #929000632103 Philips).
755 Wild-type (WT) plants in all experiments were Arabidopsis thaliana L. (Heyn) accession
756 Ler-0. The At*fer-2* mutant was obtained from the Signal Collection at the Salk Institute.
757 Plants were grown in soil (ED73; Universalerde), covered with a thin quartz sand layer,
758 under long photoperiods (16 hs light/8 hs dark) at 23°C and 60% relative humidity.

759

760 ## METHOD DETAILS

761 **Phylogenetic analysis**

762 Protein sequences were identified in plant genomes via BLASTp searches in
763 https://phytozome.jgi.doe.gov/pz/portal.html. To elucidate the evolutionary relationship
764 across land plant evolutionary history, we focused on *A. thaliana, Selaginella*

765 *moellendorffii, Physcomitrella patens* and *M. polymorpha*, as representative species for
766 angiosperms, lycophytes, mosses and liverworts, respectively. Complete or partial coding
767 protein sequences were aligned using the ClustalW parameters and were conducted in
768 MEGA7. Phylogenetic trees were constructed with Neighbor-joining method, with a
769 bootstrap test of 1000 replicates. The evolutionary distances were computed using the
770 Poisson correction method.
771
772 **Vector construction**
773 Expression constructs: a BJ36 plasmid [77] containing a tripleVENUS-NLS (trpVNS)
774 fragment was modified by adding a ligation-independent cloning (LiC) adapter site [78].
775 A promoter fragment of Mp*FER* of 3.2 kb was amplified using primers specified below
776 and cloned into the BJ36 vector via LiC cloning. $_{pro}$Mp*FER* promoter fragment fused to
777 trpVNS was then shuttled via *Not*I restriction sites into the HART01 [77] expression
778 vector. The expression vector was also directly modified to contain the LiC sites, so
779 promoter fragments can now be directly cloned in front of the trpVNS in the HART01
780 vector via LiC-cloning. This vector was called VHL (trpVNS-containing HART01 vector
781 with LiC sites).
782 amiRNA constructs: For functional analyses three independent artificial microRNA
783 (amiRNA) constructs were made (Figure S2). The endogenous microRNA precursor
784 Mp*miR160* was used as both backbone and template to design the constructs which
785 generate single species small RNA molecules of 21 nt length, complementary to the
786 target gene transcript [63,79]. Three miR160 backbones containing independent amiR-
787 Mp*FER*/amiR-Mp*FER** duplexes were synthesized by GenScript and fused to the
788 $_{pro}$Mp*EF1* promoter in the BJ36 shuttle vector and shuttled to the HART01 expression
789 vector as described previously [79]. The folding structure and design procedures were

790 explained in detail in [63,79]. The sequences for the amiRNAs were designed to retain
791 the exact physical properties of the endogenous Mp*miR160* template. The folding
792 patterns were analyzed in the Mfold software [80] and the sequences synthesized (Figure
793 S2).
794 CRISPR/Cas gRNA: Selection of target sites was done using CasFinder [81].
795 Complementary oligos were designed and annealed for ligation into gRNA, in the
796 pMpGE_En03 vector, previously digested with BsaI restriction enzyme. Resulting gRNAs
797 were incorporated into binary vector pMpGE011 through gateway recombination.
798 Over-expression of Mp*FER* and At*FER*: The full-length Mp*FER* sequence was amplified
799 from genomic *M. polymorpha* DNA with attB sites and Gateway-cloned via pDONR207.
800 For *A. thaliana* expression, Mp*FER* was introduced into the expression vectors
801 pMDC201, which contains a *2X35S* promoter fragment and an in-frame C-terminal
802 mGFP6 [82]. For *M. polymorpha* expression, Mp*FER* was introduced intro the binary
803 vector pMpGWB308, which contains a MpEF1 promoter and an in-frame C-terminal
804 citrine [83]. Similarly, for expression of At*FER* in *M. polymorpha*, coding sequence of
805 AtFER was introduced into pMpGWB308 binary vector, for the generation of
806 $_{pro}$Mp*EF1:*At*FER-Cit* construct.
807

808 **Quantitative real-time PCR (qRT-PCR) and droplet digital PCR (ddPCR)**

809 RNA extraction from *M. polymorpha*: RNA extraction from thallus tissue (ca. 100mg
810 including apical notch) was done using the Rneasy plant mini kit (#74904, Qiagen). To
811 remove contaminating DNA, the TURBO DNAfree™ Kit (AM1907 Ambion) was used
812 according to manufacturer's recommendations. To extract RNA from the gametophores
813 (2 antheridiophores > 5mm diameter were pooled, respectively, for each replicate), the
814 Direct(-zol) RNA MiniPrep (#R2050, ZymoResearch) was used with TRIzol Reagent

815 (#15596026, Ambion) according to the manufacturer's protocol, including on-column
816 DNase digestion and subsequent TURBO DNA-free™ Kit (AM1907 Ambion) treatment.
817 RNA samples were quantified using the Qubit® RNA HS Assay Kit (#Q32852, Life
818 Technologies), a Nanodrop ND-1000 Spectrometer or an Agilent 2100 BioAnalyzer.
819 cDNA synthesis: cDNA was synthesized from 0.5 *µ*g or 1.0 *µ*g of total RNA. Reverse
820 transcription was performed in 25 *µ*l with 20*µ*g/ml Oligo(dT) 12-18 primers and 200 units
821 of SuperScript® II Reverse Transcriptase (#18064-014, Invitrogen) according to the
822 manufacturer's protocol. The resulting cDNA was diluted 1:9 by adding nuclease-free
823 water. To control for genomic DNA contamination, control replicates of all samples were
824 incubated without SuperScript® II reverse transcriptase.
825 Primer tests and quantitative RT-PCR: Primer efficiency and concentration tests were
826 carried out for Mp*FER* and suitable reference genes as described previously (Rövekamp
827 et al., 2016, Althoff et al., 2014). Amplification experiments were carried out using a 7500
828 Applied Biosystem Fast Real-Time PCR System. Reactions were performed in 20 *µ*l
829 volumes containing 10 *µ*l 2X SYBR-green mastermix (SsoAdvanced™ Universal
830 SYBRGreen Supermix), 200 nM (Mp*EF1* and Mp*FER*) or 250 nM (Mp*ACTIN*) forward and
831 reverse primers, and 1 *µ*l diluted cDNA. Where possible, three technical and biological
832 replicates were performed for each reaction. The primers used for the qRT-PCR are
833 summarized in Table S1.
834 For ddPCR analysis, individual PCR reactions were performed in a total volume of 25 *µ*l,
835 using 1X ddPCR EvaGreen Supermix, with droplets generated according to
836 manufacturer's recommendations. Reading of the PCR-amplified droplets was carried out
837 by the QX200 Droplet Reader (Bio-Rad) and analysed by the QuantaSoft TM Software
838 (v1.4, Bio-Rad). The counts from ddPCR were normalised through a log2 transformation.
839 Afterwards, relative expression was calculated against the geometric mean of the counts

840 for all three reference genes (Mp*ACT1*, Mp*ACT7*, and Mp*APT3*) [84]: (log2(gene tested
841 + 1) - log2(geom. mean of all references + 1)). The primers used for the ddPCR are
842 summarized in Table S1.
843
844 **Transformation into *M. polymorpha* and *A. thaliana***
845 *Agrobacterium*-mediated transformation using regenerating thalli of *M. polymorpha* was
846 done by co-cultivation 15-days old Marchantia fragments with transformed *Agrobacterium*
847 *tumefaciens* (GV3101) cells [85,86]. After three days of incubation, positive transformants
848 were selected on Gamborg's B5 plates supplemented with 10 *µ*g/ml Hygromicin B
849 (Invitrogen), 0.5 µM Chlorosulfuron or Kanamycin, and 100 µg/ml of Cefotaxime sodium.
850 Isogenic lines were obtained by using plants derived from gemmae of the T1 generation
851 (G1 generation). G1 or subsequent gemmae generations were used for all experiments,
852 as they are derived from single cells [87,88]. Transformation of *A. thaliana* via *A.*
853 *tumefaciens* (GV3101) was performed by floral dipping according to [89]. Primers used
854 for amplification of promoter fragments of Mp*FER* are listed in Table S2.
855
856 **Microscopy**
857 Plants were observed in a Lumar.V12 (Zeiss) or a Leica MZFLIII dissection microscope
858 and photographed with an AxioCam HRc (Zeiss) or Leica DFC 420C camera. Clearings
859 were observed using a Leica DMR microscope and photographed with an Axiocam 105
860 color camera. Fluorescence reporter expression were analyzed using a Leica SP5
861 confocal microscope. Fiji [90] and GIMP (version 2.8.10) software were used for
862 adjustments of brightness, contrast, channel selection, and image size.
863 Tissue clearing for bright field microscopy: *M. polymorpha* tissues were fixed in Carnoy's
864 solution and incubated at 4$^{o}$C overnight, followed by rehydration in an ethanol series of

865 85%, 70%, 50%, and 30%. Samples were incubated for 1 hour at 4°C for each step and
866 then incubated in chloral hydrate solution at 4°C overnight. Samples were mounted in
867 chloral hydrate.
868 Calcofluor-white staining for cell size measurements: Pieces of fresh thallus tissue
869 located in fully differentiated zones [91] of plants grown on plates were dissected out and
870 put into water. The pieces were transferred to PBS pH 6.1 containing 100 *µ*g/ml
871 Calcofluor-white and vacuum-infiltrated for 1 hour before being mounted on slides. The
872 area of the epidermal cells was measured using Imaris 8.3.1. software. Cells of air pores
873 and the two adjacent cell layers were excluded from the analysis, as well as the spiralling
874 cells surrounding newly developing air pores.
875 For cell-death staining, seven-days old gemmalings were stained with lactophenol-
876 trypanblue (10 mL of lactic acid, 10 mL of glycerol, 10 g of phenol, 10 mg of trypan blue,
877 dissolved in 10 mL of distilled water) and boiled for approximately 1 min in the stain
878 solution and then decolorized in chloral hydrate (2.5 g of chloral hydrate dissolved in 1
879 mL of distilled water) for at least 30 min. They were mounted in chloral hydrate and
880 imaged in dissecting microscope.
881
882 **Western blot analysis**
883 *M. polymorpha* explants were ground in liquid nitrogen and resuspended in 300 µL of
884 Laemmli buffer [92]. After centrifugation at 6,000 rpm for 5 min at 4˚C, the supernatant
885 was recovered. Protein accumulation was confirmed by Western blotting, using the anti-
886 GFP antibody (1:3000, Torrey Pines Biolabs). As secondary antibodies, the Agrisera
887 S09602 goat anti-rabbit antibody was used with the ECL-chemistry of FUSION FX -
888 Western Blot & Chemi Imaging (Vilber Lourmat).
889

890 **Growth rate experiments**

891 Gemmae of wild-type, Mp*fer-1*, and independent transformation lines of amiR-Mp*FER*
892 lines were grown on plates and the thallus area was measured over time. 10 or 30
893 gemmae of four independent transformation lines were grown on half-strength Gamborg's
894 B5 and scanned on an Epson 2450 Photo scanner at 600dpi. Plant area was measured
895 using color threshold settings and particle analysis in the Fiji software [90].

896

897 **Expression map**

898 Gene expression of *Cr*RLK1L signaling pathway components was calculated from
899 publicly available RNA-seq data of 39 samples of *M. polymorpha* Tak-1 and Tak.2.
900 Samples were grouped by tissue and analyzed under the same pipeline: Nextera paired-
901 end adapters were trimmed from sequencing reads using the bbduk tool embedded in
902 the BBMap software package [93]. Read ends with quality below 20 were also trimmed
903 and the minimum read length was set to 25. The rest of parameters of bbduk were set as
904 default. Reads were mapped to *M. polymorpha* reference genome (v3.1) [45] using the
905 Tophat software (v2.1.1) [94], designed for RNA-sequencing read mapping. Tophat
906 contains Bowtie (v2.3.2.0) [95] as the aligner software. All parameters were set to default
907 values except for the RAM memory and number of used Cores. Mapped reads were
908 sorted using samtools (v1.3.1) [96] and counted with the software HTSeq-count" (v.0.9.1)
909 [97]. Gene expression values were calculated using the package DESeq2 (Release 3.6)
910 [98] for R software (v3.4.4) [99]. Another R package, ggplot2 (release 2.2.1) [100] was
911 used for producing the figures. A summary of the samples that were used in this study is
912 provided in Table S3.

913

914

915 **Three-dimensional (3D) protein structure modeling**

916 Comparative modeling of protein 3D structures was performed using the SWISS-MODEL
917 online-tool [60]. The software was fed with the three protein sequences of MpFER,
918 MpRALF1, and MpLRE1 as input to model, and one PDB file as a 3D template, which
919 contains the published crystal structure of the protein complex formed by AtFER,
920 AtRALF23, and AtLLG2 [35]. Quality control of the model was assessed using the same
921 tool and the results are summarized in Figure S5E. Spatial comparisons of the *M.*
922 *polymorph*a predicted structures with the crystal structures of *A. thaliana* were performed
923 in PyMol [101].

924

925 ## QUANTIFICATION AND STATISTICAL ANALYSIS

926 Analyses were performed in InfoStat (http://www.infostat.com.ar). Tests are indicated in
927 the corresponding figure legend.

928

929 ## References


930 1. Showalter AM. (1993). Structure and function of plant cell wall proteins. Plant Cell *5*, 9–23.

931 2. Franck CM, Westermann J, Boisson-Dernier A. (2018). Plant malectin-like receptor kinases: from cell
932 wall integrity to immunity and beyond. Annu Rev Plant Biol *69*, 301–328.

933 3. Shiu SH, Bleecker AB. (2001). Plant receptor-like kinase gene family: diversity, function, and
934 signaling. Sci STKE *2001*, re22.

935 4. Steinwand BJ, Kieber JJ. (2010). The role of receptor-like kinases in regulating cell wall function.
936 Plant Physiol. *153*, 479–84.

937 5. Wolf S, Hématy K, Hofte H. (2012). Growth control and cell wall signaling in plants. Annu Rev Plant
938 Biol *63*, 381–407.

939 6. Escobar-Restrepo J-M, Huck N, Kessler S, Gagliardini V, Gheyselinck J, et al. (2007). The FERONIA
940 receptor-like kinase mediates male-female interactions during pollen tube reception. Science *317*,
941 656–660.

942 7. Hématy K, Sado PE, Van Tuinen A, Rochange S, Desnos T, et al. (2007). A receptor-like kinase
943 mediates the response of *Arabidopsis* cells to the inhibition of cellulose synthesis. Curr Biol. *17*,
944 922–931.

945 8. Boisson-Dernier A, Roy S, Kritsas K, Grobei MA, Jaciubek M, Schroeder, J.I., Grossniklaus, U. (2009).
946 Disruption of the pollen-expressed *FERONIA* homologs *ANXUR1* and *ANXUR2* triggers pollen tube
947 discharge. Development *136*, 3279–3288.

948 9. Guo H, Li L, Ye H, Yu X, Algreen A, Yin Y. (2009). Three related receptor-like kinases are required for
949 optimal cell elongation in *Arabidopsis thaliana*. Proc Natl Acad Sci USA *106*, 7648–7653.

950 10. Guo H, Ye H, Li L, Yin Y. (2009). A family of receptor-like kinases are regulated by *BES1* and involved
951 in plant growth in *Arabidopsis thaliana*. Plant Signal Behav *4*, 784–786.

952 11. Kessler SA, Shimosato-Asano H, Keinath NF, Wuest SE, Ingram G, et al. (2010). Conserved molecular
953 components for pollen tube reception and fungal invasion. Science *330*, 968–971.

954 12. Bai L, Ma X, Zhang G, Song S, Zhou Y, et al. (2014). A receptor-like kinase mediates ammonium
955 homeostasis and is important for the polar growth of root hairs in *Arabidopsis*. Plant Cell *26*, 1497–
956 511.

957 13. Schoenaers S, Balcerowicz D, Breen G, Hill K, Zdanio M, Mouille G, Holman TJ, Oh J, Wilson MH, et
958 al., (2018). The auxin-regulated *Cr*RLK1L kinase ERULUS controls cell wall composition during root
959 hair tip growth. Curr. Biol. *28*, 722–732.

960 14. Miyazaki S, Murata T, Sakurai-Ozato N, Kubo M, Demura T, et al. (2009). *ANXUR1* and *2*, sister
961 genes to *FERONIA*/*SIRENE*, are male factors for coordinated fertilization. Curr Biol. *19*, 1327–1331.

962 15. Keinath NF, Kierszniowska S, Lorek J, Bourdais G, Kessler SA, Shimosato-Asano H, Grossniklaus U,
963 Schulze WX, Robatzek S, Panstruga RJ (2010). PAMP (pathogen-associated molecular pattern)-
964 induced changes in plasma membrane compartmentalization reveal novel components of plant
965 immunity. J Biol Chem *285*, 39140–39149.

966 16. Duan Q, Kita D, Li C, Cheung AY, Wu HM. (2010). FERONIA receptor-like kinase regulates RHO
967 GTPase signaling of root hair development. Proc Natl Acad Sci USA *107*, 17821–17826.

968 17. Galindo-Trigo S, Blanco-Touriñán N, DeFalco TA, Wells ES, Gray JE, Zipfel C, Smith LM. (2020).
969 *Cr*RLK1L receptor-like kinases HERK1 and ANJEA are female determinants of pollen tube reception.
970 EMBO Rep *21*, e48466.

971 18. Zhu L, Chu LC, Liang Y, Zhang XQ, Chen LQ, Ye D. (2018). The *Arabidopsis Cr*RLK1L protein kinases
972 BUPS1 and BUPS2 are required for normal growth of pollen tubes in the pistil. Plant J *95*, 474–486.

973 19. Li C, Yeh F-L,Cheung AY, Duan Q, KitaD, et al. (2015). Glycosylphosphatidylinositol-anchored
974 proteins as chaperones and co-receptors for FERONIA receptor kinase signaling in *Arabidopsis*. eLife
975 *4*, e06587.

976 20. Richter J, Ploderer M, Mongelard G, Gutierrez L, Hauser MT. (2017). Role of *Cr*RLK1L cell wall
977 sensors HERCULES1 and 2, THESEUS1, and FERONIA in growth adaptation triggered by heavy metals
978 and trace elements. Front Plant Sci *8*, 1554.

979 21. Richter J, Watson JM, Stasnik P, Borowska M, Neuhold J, Berger M, Stolt-Bergner P, Schoft V,
980 Hauser MT. (2018). Multiplex mutagenesis of four clustered *Cr*RLK1L with CRISPR/Cas9 exposes
981 their growth regulatory roles in response to metal ions. Sci Rep *8*, 12182.

982 22. Stegmann M, Monaghan J, Smakowska-Luzan E, Rovenich H, Lehner A, et al. (2017). The receptor
983 kinase FER is a RALF-regulated scaffold controlling plant immune signaling. Science *355*, 287–289.

984 23. Ngo QA, Vogler H, Lituiev DS, Nestorova A, Grossniklaus U. (2014). A calcium dialog mediated by
985 the *FERONIA* signal transduction pathway controls plant sperm delivery. Dev Cell *29*, 491–500.

986 24. Yu F, Qian L, Nibau C, Duan Q, Kita D, et al. (2012). *FERONIA* receptor kinase pathway suppresses
987 abscisic acid signaling in *Arabidopsis* by activating ABI2 phosphatase. Proc Natl Acad Sci USA *109*,
988 14693–14698.

989 25. Mao D, Yu F, Li J, Van de Poel B, Tan D, et al. (2015). FERONIA receptor kinase interacts with S-
990 adenosylmethionine synthetase and suppresses S-adenosylmethionine production and ethylene
991 biosynthesis in *Arabidopsis*. Plant Cell Env. *38*, 2566–2574.

992 26. Deslauriers SD, Larsen PB. (2010). *FERONIA* is a keymodulator of brassinosteroid and ethylene
993 responsiveness in *Arabidopsis* hypocotyls. Mol Plant *3*, 626–640.

994 27. Shih H-W, Miller ND, Dai C, Spalding EP, Monshausen GB. (2014). The receptor-like kinase FERONIA
995 is required for mechanical signal transduction in *Arabidopsis* seedlings. Curr Biol. *24*, 1887–1892.

996 28. Denness L, McKenna JF, Segonzac C, Wormit A, Madhou P, et al. (2011). Cell wall damage-induced
997 lignin biosynthesis is regulated by a reactive oxygen species- and jasmonic acid-dependent process
998 in *Arabidopsis*. Plant Physiol *156*, 1367–1374.

999 29. Okuda S, Tsutsui H, Shiina K, Sprunck S, Takeuchi H, Yui R, Kasahara RD, Hamamura Y, Mizukami A,
1000 Susaki D, Kawano N, Sakakibara T, Namiki S, Itoh K, Otsuka K, Matsuzaki M, Nozaki H, Kuroiwa T,
1001 Nakano A, Kanaoka MM, Dresselhaus T, Sasaki N, Higashiyama T. (2009). Defensin-like polypeptide
1002 LUREs are pollen tube attractants secreted from synergid cells. Nature *458*, 357–361.

1003 30. Huck N, Moore JM, Federer M, Grossniklaus U. (2003). The *Arabidopsis* mutant *feronia* disrupts the
1004 female gametophytic control of pollen tube reception. Development *130*, 2149–2159.

1005 31. Rotman N, Rozier F, Boavida L, Dumas C, Berger F, Faure J-E. (2003). Female control of male gamete
1006 delivery during fertilization in *Arabidopsis thaliana*. Curr Biol. *13*, 432–436.

1007 32. Ge Z, Bergonci T, Zhao Y, Zou Y, Du S, et al. (2017). *Arabidopsis* pollen tube integrity and sperm
1008 release are regulated by RALF-mediated signaling. Science *358*, 1596–1600.

1009 33. Haruta M, Sabat G, Stecker K, Minkoff BB, Sussman MR. (2014). A peptide hormone and its receptor
1010 protein kinase regulate plant cell expansion. Science *343*, 408–411.

1011 34. Dünser K, Gupta S, Herger A, Feraru MI, Ringli C, Kleine-Vehn J. (2019). Extracellular matrix sensing
1012 by FERONIA and Leucine-Rich Repeat Extensins controls vacuolar expansion during cellular
1013 elongation in *Arabidopsis thaliana*. EMBO J *38*, pii: e100353.

1014 35. Xiao Y, Stegmann M, Han Z, DeFalco TA, Parys K, Xu L, Belkhadir Y, Zipfel C, Chai J. (2019).
1015 Mechanisms of RALF peptide perception by a heterotypic receptor complex. Nature *572*, 270–274.

1016 36. Mecchia MA, Santos-Fernandez G, Duss NN, Somoza SC, Boisson-Dernier A, et al. (2017). RALF4/19
1017 peptides interact with LRX proteins to control pollen tube growth in *Arabidopsis*. Science *358*,
1018 1600–1603.

1019 37. Capron A, Gourgues M, Neiva LS, Faure J-E, Berger F, Pagnussat G, Krishnan A, Alvarez-Mejia C,
1020 Vielle-Calzada JP, Lee YR, Liu B, Sundaresan V. (2008). Maternal control of male-gamete delivery in
1021 *Arabidopsis* involves a putative GPI-anchored protein encoded by the *LORELEI* gene. Plant Cell *20*,
1022 3038–3049.

1023 38. Boisson-Dernier A, Kessler SA, Grossniklaus U. (2011). The walls have ears: the role of plant
1024 *Cr*RLK1Ls in sensing and transducing extracellular signals. J Exp Bot *62*.

1025 39. Hématy K, Höfte H. (2008). Novel receptor kinases involved in growth regulation. Curr Opin Plant
1026 Biol. *11*, 321–328.

1027 40. Cheung AY, Wu HM. (2011). THESEUS 1, FERONIA and relatives: a family of cell wall-sensing
1028 receptor kinases? Curr Opin Plant Biol *14*, 632–641.

1029 41. Nissen KS, Willats WGT, Malinovsky FG. (2016). Understanding *Cr*RLK1L function: cell walls and
1030 growth control. Trends Plant Sci *21*, 516–527.

1031 42. Feng W, Kita D, Peaucelle A, Cartwright HN, Doan V, Duan Q, Liu MC, Maman J, Steinhorst L,
1032 Schmitz-Thom I, Yvon R, Kudla J, Wu HM, Cheung AY, Dinneny JR. (2018). The FERONIA receptor
1033 kinase maintains cell-wall integrity during salt stress through $Ca^{2+}$ signaling. Curr Biol. *28*, 666–675.

1034 43. Lindner H, Müller LM, Boisson-Dernier A, Grossniklaus U. (2012). *Cr*RLK1L receptor-like kinases: not
1035 just another brick in the wall. Curr Opin Plant Biol *15*, 656–669.

1036 44. Galindo-Trigo S, Gray JE, Smith LM. (2016). Conserved roles of *Cr*RLK1L receptor-like kinases in cell
1037 expansion and reproduction from algae to angiosperms. Front Plant Sci *7*, 1269.

1038 45. Bowman JL, Kohchi T, Yamato KT, Jenkins J, Shu S, Ishizaki K, et al. (2017). Insights into land plant
1039 evolution garnered from the *Marchantia polymorpha* genome. Cell *171*, 287-304.e15.

1040 46. Rövekamp M, Bowman JL, Grossniklaus U. (2014). Back to the rhizoids of plant sexual development.
1041 Abstr. 23rd Intl. Congr. Sex. Plant Reprod. Porto Port.,
1042 https://www.fc.up.pt/sprporto2014/doc/23rd%20International%20congress%20on%20sexual%20p
1043 lant%20reproduction%20ABSBook.pdf.

1044 47. Bowman JL, Floyd SK, Sakakibara K (2007). Green genes-comparative genomics of the green branch
1045 of life. Cell *129*, 229–234.

1046 48. Nishiyama T, Fujita T, Shin-I T, Seki M, Nishide H, Uchiyama I, Kamiya A, Carninci P, Hayashizaki Y,
1047 Shinozaki K, et al. (2003). Comparative genomics of *Physcomitrella patens* gametophytic
1048 transcriptome and *Arabidopsis thaliana*: implication for land plant evolution. Proc Natl Acad Sci USA
1049 *100*, 8007–8012.

1050 49. Qiu YL, Li L, Wang B, Chen Z, Knoop V, Groth-Malonek M, Dombrovska O, Lee J, Kent L, Rest J, et al.
1051 (2006). The deepest divergences in land plants inferred from phylogenomic evidence. Proc Natl
1052 Acad Sci USA *103*, 15511–15516.

1053 50. Wickett NJ, Mirarab S, Nguyen N, Warnow T, Carpenter E, Matasci N, Ayyampalayam S, Barker MS,
1054 Burleigh JG, Gitzendanner MA, et al. (2014). Phylotranscriptomic analysis of the origin and early
1055 diversification of land plants. Proc Natl Acad Sci USA *1111*, E4859–E4868.

1056 51. Mishler BD, Churchill SP (1984). A cladistic approach to the phylogeny of the "bryophytes."
1057 Brittonia *36*, 406–424.

1058 52. Kenrick P, Crane PR (1997). The origin and early evolution of plants on land. Nature *389*, 33–39.

1059 53. Floyd SK, Bowman JL. (2007). The ancestral developmental tool kit of land plants. Int J Plant Sci *168*,
1060 1–35.

1061 54. Bowman JL, Araki T, Arteaga-Vazquez MA, Berger F, Dolan L, Haseloff J, Ishizaki K, Kyozuka J, Lin SS,
1062 Nagasaki H, Nakagami H, Nakajima K, Nakamura Y, Ohashi-Ito K, Sawa S, Shimamura M, Solano R,
1063 Tsukaya H, Ueda T, Watanabe Y, Yamato KT, Zachgo S, Kohchi T (2016). The naming of names:
1064 guidelines for gene nomenclature in *Marchantia*. Plant Cell Physiol *57*, 257–261.

1065 55. Ishizaki K (2017). Evolution of land plants: insights from molecular studies on basal lineages. Biosci
1066 Biotechnol Biochem *81*, 73–80.

1067 56. Honkanen S, Jones VAS, Morieri G, Champion C, Hetherington AJ, Kelly S, Proust H, Saint-Marcoux
1068 D, Prescott H, Dolan L. (2016). The mechanism forming the cell surface of tip-growing rooting cells
1069 Is conserved among land plants. Curr Biol. *26*, 3238–3244.

1070 57. Westermann J, Streubel S, Franck CM, Lentz R, Dolan L, Boisson-Dernier A. (2019). An evolutionarily
1071 conserved receptor-like kinases signaling module controls cell wall integrity during tip growth. Curr
1072 Biol. *29*, 4153.

1073 58. Kessler SA, Lindner H, Jones DS, Grossniklaus U. (2014). Functional analysis of related *Cr*RLK1L
1074 receptor-like kinases in pollen tube reception. EMBO Rep *16*, 107–115.

1075 59. Hirano N, Marukawa Y, Abe J, Hashiba S, Ichikawa M, Tanabe Y, (2015). A receptor-like kinase,
1076 related to cell wall sensor of higher plants, is required for sexual reproduction in the unicellular
1077 Charophycean alga, *Closterium peracerosum–strigosum– littorale* Complex. Plant Cell Physiol *56*,
1078 1456–1462.

1079 60. Schwede T, Kopp J, Guex N, Peitsch MC (2003). SWISS-MODEL: an automated protein homology-
1080 modeling server. Nucleic Acids Res. *31*, 3381–3385.

1081 61. Liu L, Zheng C, Kuang B, Wei L, Yan L, Wang T (2016). Receptor-like kinase RUPO interacts with
1082 potassium transporters to regulate pollen tube growth and integrity in rice. PLoS Genet *12*,
1083 e1006085.

1084 62. Schulze-Muth P, Irmler S, Schröder G, Schröder J (1996). Novel type of receptor-like protein kinase
1085 from a higher plant (*Catharanthus roseus*): cDNA, gene, intramolecular autophosphorylation, and
1086 identification of a threonine important for auto- and substrate phosphorylation. J Biol Chem *271*,
1087 26684–26689.

1088 63. Flores-Sandoval E, Dierschke T, Fisher TJ, Bowman JL (2016). Efficient and inducible use of artificial
1089 microRNAs in *Marchantia polymorpha*. Plant Cell Physiol *57*, 281–290.

1090 64. Althoff F, Kopischke S, Zobell O, Ide K, Ishizaki K, Kohchi T, Zachgo S. (2014). Comparison of the
1091 Mp*EF1α* and CaMV35 promoters for application in *Marchantia polymorpha* overexpression studies.
1092 Transgenic Res. *23*, 235–244.

1093 65. Gonneau M, Desprez T, Martin M, Doblas VG, Bacete L, Miart F, Sormani R, Hématy K, Renou J,
1094 Landrein B et al. (2018). Receptor kinase THESEUS1 is a RAPID ALKALINIZATION FACTOR34 receptor
1095 in *Arabidopsis*. Curr Biol. *28*, 2452–2458.

1096 66. Gachomo EW, Jno Baptiste L, Kefela T, Saidel WM, Kotchoni SO (2014). The *Arabidopsis CURVY1*
1097 (*CVY1*) gene encoding a novel receptor-like protein kinase regulates cell morphogenesis, flowering
1098 time and seed production. BMC Plant Biol *14*, 221.

1099 67. Merz D, Richter J, Gonneau M, Sanchez-Rodriguez C, Eder T, Sormani R, Martin M, Hématy K, Höfte
1100 H, Hauser MT (2017). T-DNA alleles of the receptor kinase THESEUS1 with opposing effects on cell
1101 wall integrity signaling. J Exp Bot *68*, 4583–4593.

1102 68. Chiyoda S, Ishizaki K, Kataoka H, Yamato KT, Kohchi T (2008). Direct transformation of the liverwort
1103 *Marchantia polymorpha* L. by particle bombardment using immature thalli developing from spores.
1104 Plant Cell Rep *27*, 1467–1473.

1105 69. Srivastava R, Liu JX, Guo H, Yin Y, Howell SH (2009). Regulation and processing of a plant peptide
1106 hormone, AtRALF23, in *Arabidopsis*. Plant J *59*, 930–939.

1107 70. Boisson-Dernier A, Franck CM, Lituiev DS, Grossniklaus U. (2015). Receptor-like cytoplasmic kinase
1108 MARIS functions downstream of *Cr*RLK1L-dependent signaling during tip growth. Proc Natl Acad Sci
1109 USA *112*, 12211–12216.

1110 71. Liao H-Z, Zhu M-M, Cui H-H, Du X-Y, Tang Y, et al. (2016). *MARIS* plays important roles in
1111 *Arabidopsis* pollen tube and root hair growth. J Integr Plant Biol *58*, 927–940.

1112 72. Bowen EJ (1935). A note on the conduction of water in *Fimbriaria bleumeana*. Ann. Bot. *49*, 844–
1113 848.

1114 73. Fujikura U, Elsaesser L, Breuninger H, Sánchez-Rodríguez C, Ivakov A, Laux T, Findlay K, Persson S,
1115 Lenhard M. (2014). Atkinesin-13A modulates cell-wall synthesis and cell expansion in *Arabidopsis*
1116 *thaliana* via the *THESEUS1* pathway. PLoS Genet *10*, e1004627.

1117 74. Pierik R, Tholen D, Poorter H, Visser EJ, Voesenek LA (2006). The Janus face of ethylene: growth
1118 inhibition and stimulation. Trends Plant Sci *11*, 176–183.

1119 75. Wolf S, Höfte H. (2014). Growth control: a saga of cell walls, ROS, and peptide receptors. Plant Cell
1120 *26*, 1848–1856.

1121 76. Humplík JF, Bergougnoux V, Van Volkenburgh E (2017). To stimulate or inhibit? That Is the question
1122 for the function of abscisic acid. Trends Plant Sci *22*, 830–841.

1123 77. Flores-Sandoval E, Eklund DM, Bowman, JL (2015). A simple auxin transcriptional response system
1124 regulates multiple morphogenetic processes in the liverwort *Marchantia polymorpha*. PLoS Genet
1125 *11*, e1005207.

1126 78. De Rybel B, van den Berg W, Lokerse AS., Liao C-Y, van Mourik H, Moller B, Llavata-Peris CI, Weijers
1127 D (2011). A versatile set of ligation-independent cloning vectors for functional studies in plants.
1128 Plant Physiol. *156*, 1292–1299.

1129 79. Rövekamp M, Bowman JL, Grossniklaus U (2016). *Marchantia* Mp*RKD* regulates the gametophyte-
1130 sporophyte transition by keeping egg cells quiescent in the absence of fertilization. Curr. Biol. *26*,
1131 1782–1789.

1132 80. Zuker M. (2003). Mfold web server for nucleic acid folding and hybridization prediction. Nucleic
1133 Acids Res *31*, 3406–3415.

1134 81. Aach J, Mali P, Church GM (2014). CasFinder: flexible algorithm for identifying specific Cas9 targets
1135 in genomes. BioRxiv Doi 101101005074.

1136 82. Curtis MD, Grossniklaus U (2003). A Gateway cloning vector set for high-throughput functional
1137 analysis of genes *in planta*. Plant Physiol. *133*, 462–469.

1138 83. Ishizaki K, Nishihama R, Ueda M, Inoue K, Ishida S, Nishimura Y, Shikanai T, Kohchi T (2015).
1139 Development of Gateway binary vector series with four different selection markers for the
1140 liverwort *Marchantia polymorpha*. PLoS ONE *10*, e0138876.

1141 84. Vandesompele J, De Preter K, Pattyn F, Poppe B, Van Roy N, De Paepe A, Speleman F. (2002).
1142 Accurate normalization of real-time quantitative RT-PCR data by geometric averaging of multiple
1143 internal control genes. Genome Biol *3*, RESEARCH0034.

1144 85. Kubota A, Ishizaki K, Hosaka M, Kohchi T (2013). Efficient *Agrobacterium*-mediated transformation
1145 of the liverwort *Marchantia polymorpha* using regenerating thalli. Biosci Biotechnol Biochem *77*,
1146 167–172.

1147 86. Ishizaki K, Chiyoda S, Yamato KT, Kohchi, T (2008). *Agrobacterium*-mediated transformation of the
1148 haploid liverwort *Marchantia polymorpha* L., an emerging model for plant biology. Plant Cell
1149 Physiol. *49*, 1084–1091.

1150 87. Barnes CR, Land WJG. (1907). Bryological papers. I. The origin of air chambers. Bot Gaz *44*, 197–213.

1151 88. Hughes SJ (1971). On conidia of fungi, and gemmae of algae, bryophytes, and pteridophytes. Can J
1152 Bot *49*, 1319–1339.

1153 89. Bent A. (2006). *Agrobacterium* protocols. Totowa NJ Humana Press *Volume I*.

1154 90. Schindelin J, Arganda-Carreras I, Frise E, Kaynig V, Longair M, Pietzsch T, Preibisch S, et al. (2012).
1155 Fiji: An open-source platform for biological-image analysis. Nat. Methods *9*, 676–682.

1156 91. Solly JE, Cunniffe NJ Harrison CJ (2017). Regional growth rate differences specified by apical notch
1157 activities regulate liverwort thallus shape. Curr. Biol. *27*, 16–26.

1158 92. Laemmli UK (1970). Cleavage of structural proteins during the assembly of the head of
1159 bacteriophage T4. Nature *227*, 680–685.

1160 93. Bushnell B (2014). BBMap: a fast, accurate, splice-aware aligner (No. LBNL-7065E). Lawrence
1161 Berkeley Natl. LabLBNL Berkeley, CA, USA.

1162 94. Trapnell C, Pachter L, Salzberg SL (2009). TopHat: discovering splice junctions with RNA-Seq.
1163 Bioinformatics *25*, 1105–1111.

1164 95. Langdon WB (2015). Performance of genetic programming optimised Bowtie2 on genome
1165 comparison and analytic testing (GCAT) benchmarks. BioData Min. *8*, 1.

1166 96. Li H, Handsaker B, Wysoker A, Fennell T, Ruan J, Homer N, et al (2009). The sequence
1167 alignment/map format and SAMtools. Bioinformatics *25*, 2078–2079.

1168 97. Anders S, Pyl PT, Huber W. (2015). HTSeq—a Python framework to work with high-throughput
1169 sequencing data. Bioinformatics *31*, 166–169.

1170 98. Love MI, Huber W, Anders S (2014). Moderated estimation of fold change and dispersion for RNA-
1171 seq data with DESeq2. Genome Biol. *15*, 550.

1172 99. Team RC (2013). R: A language and environment for statistical computing.

1173 100. Wickham H (2016). ggplot2: elegant graphics for data analysis. *Springer*.

1174 101. DeLano WL (2002). Pymol: An open-source molecular graphics tool. CCP4 Newsl. Protein
1175 Crystallogr. *40*, 82–92.

1176

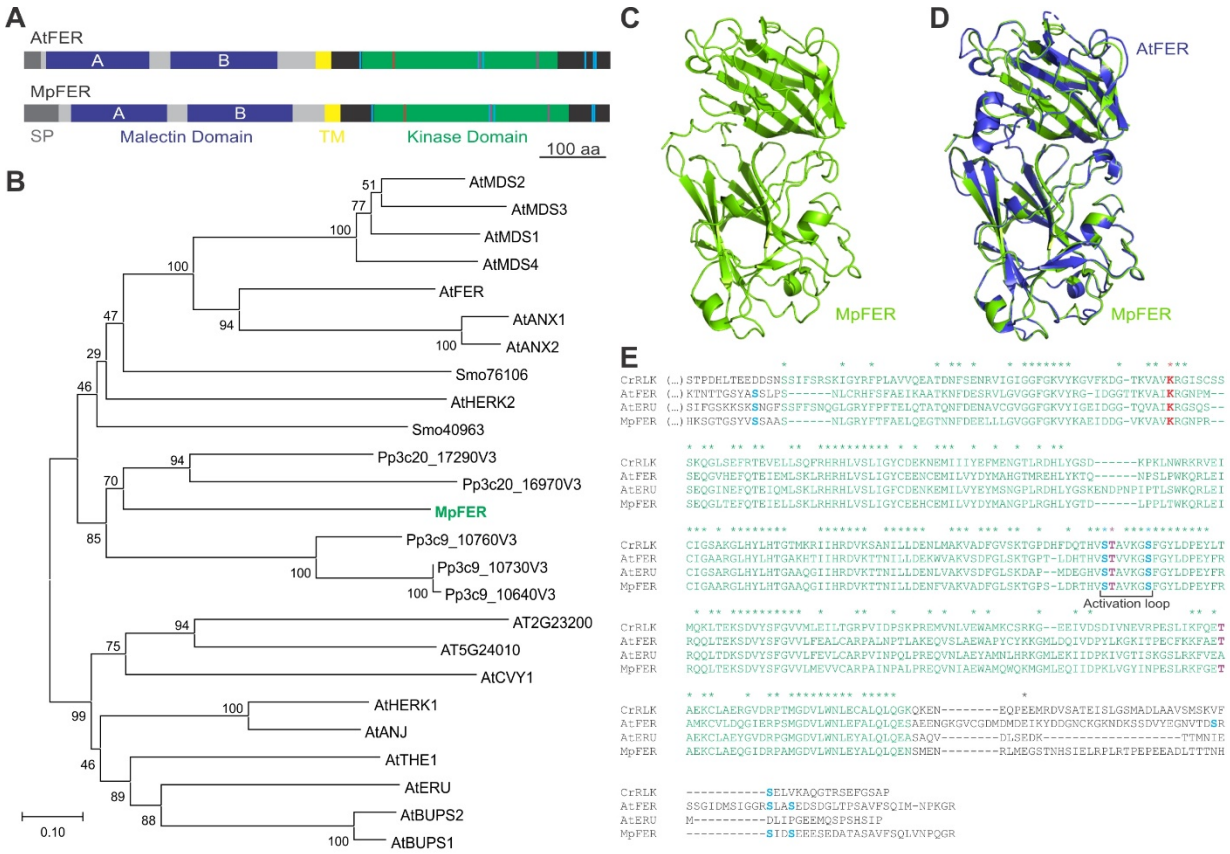


**Figure 1. *Cr*RLK1Ls Are Conserved among Land Plants**

(A) Representation of AtFER and MpFER proteins. Malectin-like domains are represented in blue and kinase domains in green. SP, signal peptide; TM, transmembrane domain (yellow). Amino acids important for regulation and activity are marked in red, violet, and light blue as described in Figure 1E.

(B) A rooted neighbor-joining tree of the amino acid sequence of the predicted malectin-like domain. *Cr*RLK1L members from *Marchantia polymorpha* (Mp), *Physcomitrella patens* (Pp), *Selaginella moellendorffii* (Smo), and *Arabidopsis thaliana* (At) were used. The numbers indicate the bootstrap values (%) from 1000 replications. The given scale represents a substitution frequency of 0.1 amino acids per site.

1190 (C) Cartoon representation of the predicted three-dimensional structure of the MpFER
1191 malectin-like domain, showing predicted alpha-helix and beta-sheet structures.
1192 (D) Structural superposition of the malectin-like domains of AtFER (blue) and MpFER
1193 (green).
1194 (E) Alignment of the cytoplasmic domains of MpFER, AtERU, AtFER, and *Cr*RLK. Kinase
1195 domains are in green, putative phosphorylation sites in light blue (Ser) and violet (Thr),
1196 and the conserved catalytic Lys in red.
1197 See also Figure S1
1198

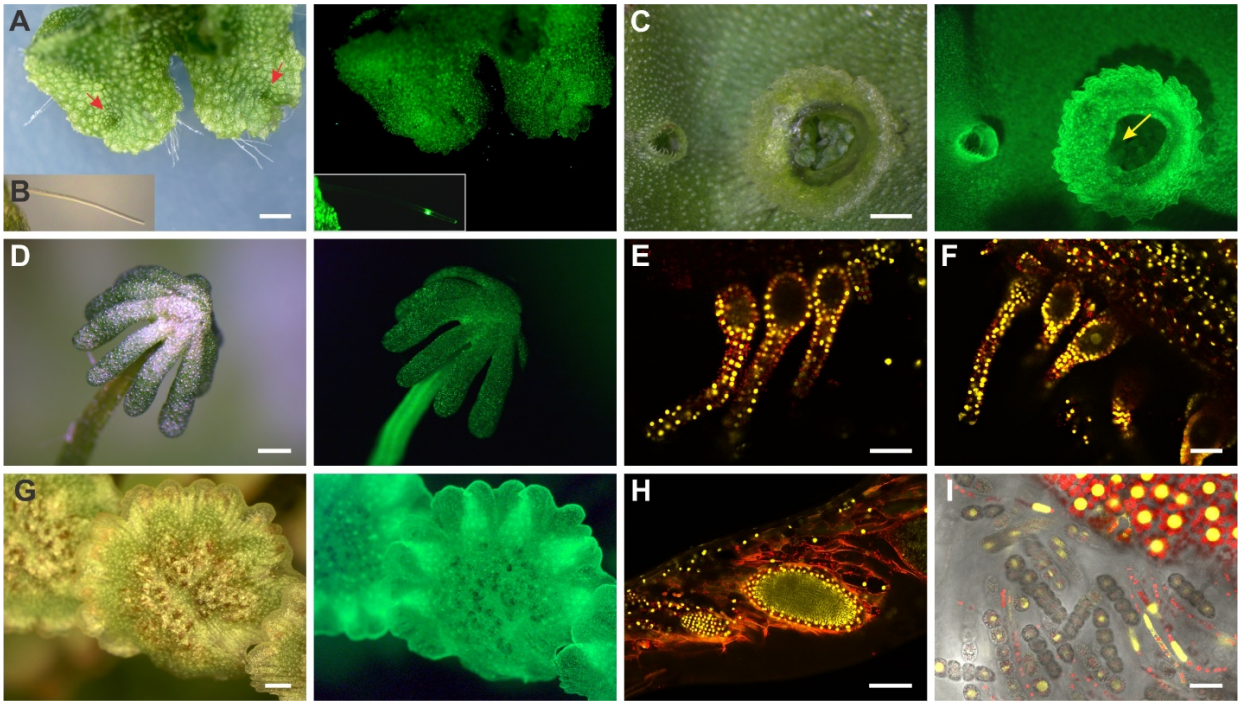


**Figure 2. Mp*FER* Is Broadly Expressed in most Tissues throughout the *M. polymorpha* Life Cycle**

Expression of $_{pro}$Mp*FER*:*trpVNS* in different organs of male and female *M. polymorpha* plants. Fluorescence is visualized as either green (epifluorescence microscope) or yellow (confocal microscope) color, depending on the panel.

(A to D) Bright field (left) and epifluorescence (right) images of a thallus, (A) rhizoid (C), gemmae cups (C), and an archegoniophore (D). Red arrows indicate meristematic zones, the yellow arrow gemmae. Scale bars, 0.5 mm.

(E and F) Confocal images of archegonia before (E) and 2 days after fertilization (F). Scale bar, 50 µm.

(G) Bright field (left) and epifluorescence (right) images of an antheridiophore. Scale bar, 1 mm.

(H) Confocal image of antheridia. Scale bar, 100 µm.

(I) Confocal image of sporophyte and spores. Scale bar, 25µm.

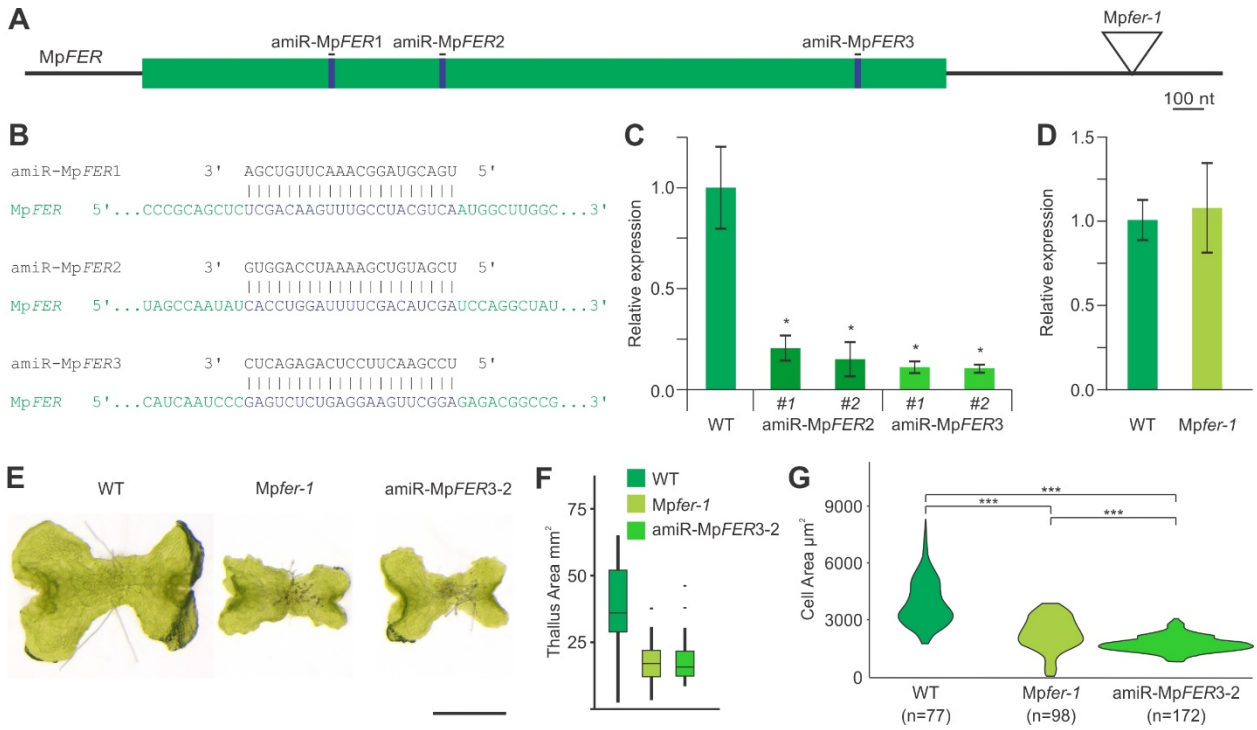


**Figure 3. Mp*FER* Controls Cell Size during Gametophyte Development**

(A) Representation of the mature Mp*FER* mRNA. Coding sequence are in green, locations of the amiRNA target sites in blue.

(B) Base complementary between mature amiR-Mp*FER*1, amiR-Mp*FER*2, and amiR-Mp*FER*3 with the Mp*FER* transcript.

(C) Relative expression level of Mp*FER* in thallus tissue from wild-type (WT; Tak1) and two independent insertion lines of amiR-Mp*FER*2 and amiR-Mp*FER*3, as measured by qRT-PCR. Mp*EF1* was used as internal control. Shown are means ± standard errors of the means (SEM) of three biological replicates. *P < 0.01, one-way analysis of variance (ANOVA).

(D) Relative expression level of Mp*FER* in WT and Mp*fer-1* thallus tissue, as measured by qRT-PCR. Mp*EF1* was used as internal control. Shown are means ± SEM of three biological replicates. *P < 0.01, one-way ANOVA.

1230 (E) Representative pictures of 10-day old gemmalings of WT, Mp*fer-1*, and amiR-
1231 Mp*FER*3-2 lines. Scale bar, 1 mm.
1232 (F) Thallus area of WT, Mp*fer-1*, and amiR-Mp*FER*3-2 lines. n = 30, outliers are indicated
1233 as black dots.
1234 (G) Violin plot of cell size in WT, *Mpfer-1*, and amiR-Mp*FER*3-2 lines. Significant
1235 differences are indicated according to the non-parametric Kruskal-Wallis test and linear
1236 regression models (***$p<0.001$).
1237 See also Figures S2 and S3
1238
1239

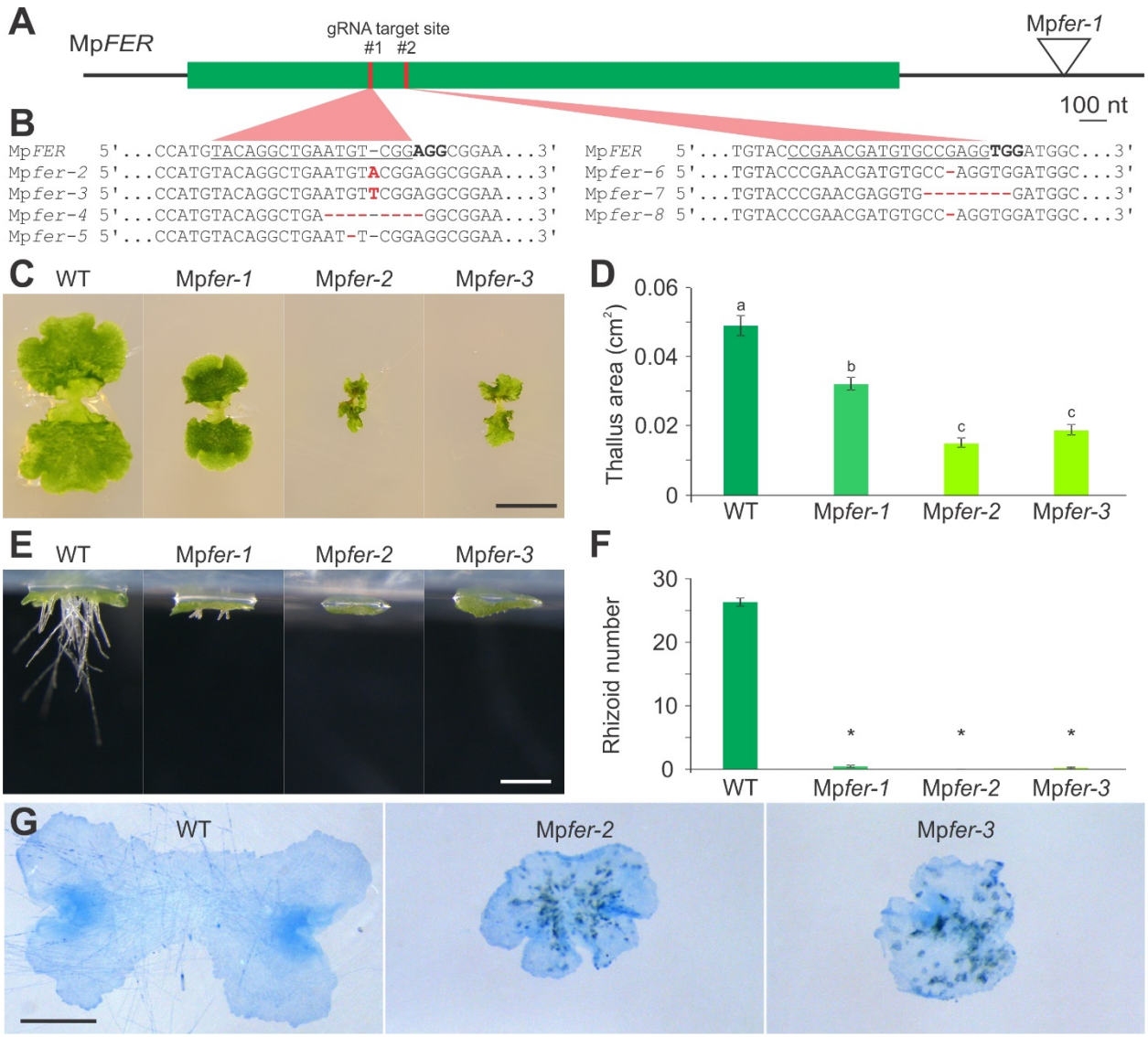


**Figure 4. The Integrity of Thalli from Mp*fer* Knock-out Lines Is Severely Affected**

(A) Representation of the mature Mp*FER* mRNA with the coding sequence in green, and the location of the gRNA target sites in red.

(B) Sequences of gRNA target sites in the confirmed Mp*fer* knock-out mutants. Deletions and insertions are highlighted in red.

(C) Representative pictures of 10-day old gemmalings of WT, Mp*fer-1*, and two independent Mp*fer* knock-out mutants. Scale bar, 0.5 cm.

1249 (D) Thallus area of 10-day old gemmalings of WT, Mp*fer-1*, and two independent Mp*fer*
1250 knock-out mutants. n = 30.
1251 (E) Representative pictures of 3-day old gemmalings growing in upside-down plates of
1252 WT, Mp*fer-1*, and two independent Mp*fer* knock-out mutants. Scale bar, 500 μm.
1253 (F) Rhizoid number in 3-day old gemmalings of WT, Mp*fer-1*, and two independent Mp*fer*
1254 knock-out mutants. n = 30.
1255 (G) Trypan blue staining of 7-days old gemmalings of WT, Mp*fer-1*, and two independent
1256 Mp*fer* knock-out mutants. Scale bar, 1 mm.
1257
1258

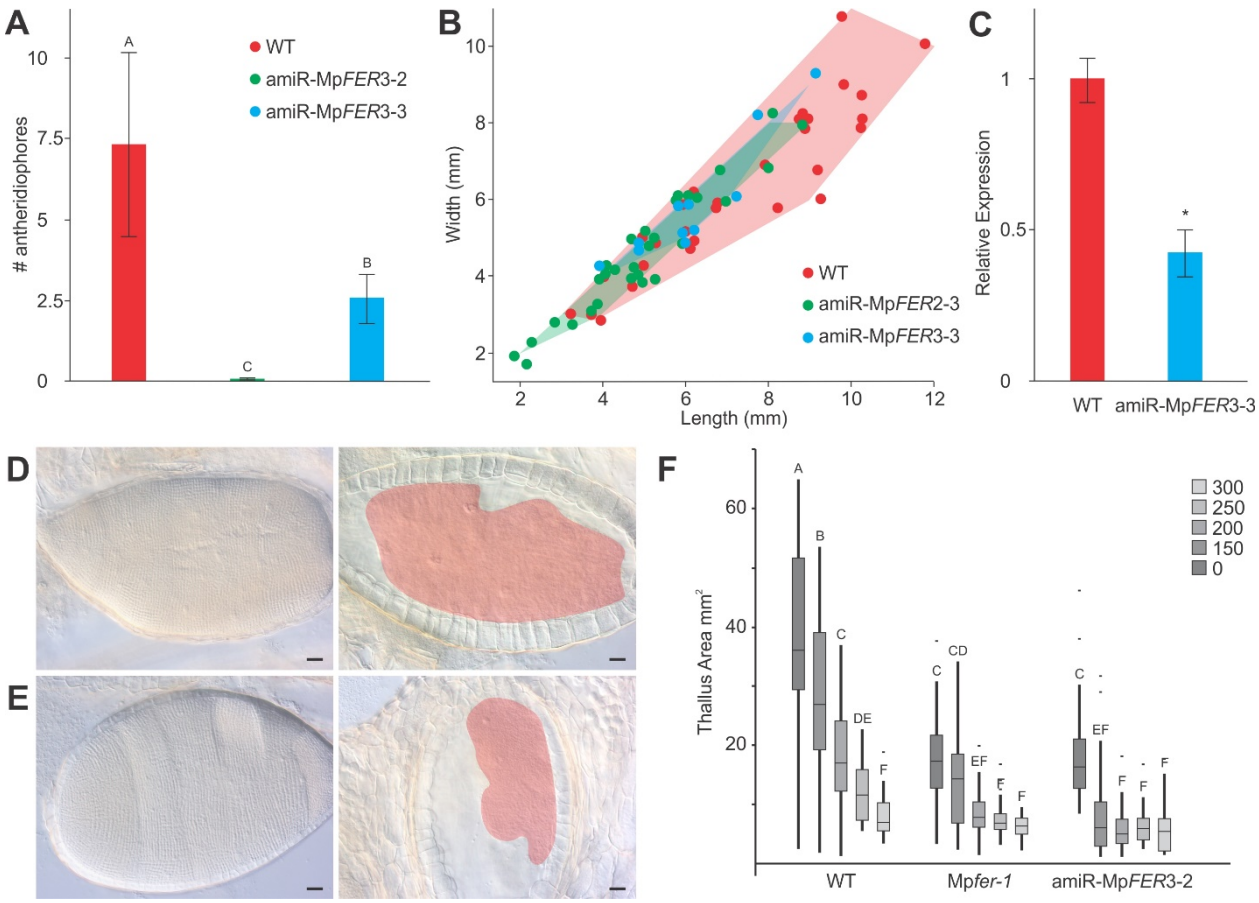


**Figure 5. Conservation of *Cr*RLK1L Function in Land Plants**

(A) Number of antheridiophores produced per plant for wild-type (WT, n=9) and two independent amiR-Mp*FER*3 lines (amiR-Mp*FER*3-2, n = 9; amiR-Mp*FER*3-3, n = 12). Shown are means ± SEM of two biological replicates. Means with same letter do not differ significant different with P > 0.05, one-way ANOVA, Duncan test.

(B) Antheridiophore splash platform size distribution of WT (n = 32), amiR-Mp*FER*2-3 (n = 34), and amiR-Mp*FER*3-3 (n = 11) lines. For all antheridia with a stalk >8 mm, length and width of the platform were recorded.

(C) qRT-PCR of Mp*FER* levels in antheridiophores in a WT and amiR-Mp*FER*3-3 line. Mp*EF1* was used as internal control. Shown are means ± SEM of three biological replicates. *P < 0.01, ANOVA.

1272 (D and E) Mature antheridia of a WT (D) and amiR-Mp*FER*3-3 line (E). Bright field images
1273 (left) and in cross-section (right). The spermatogenous areas are indicated in red. Scale
1274 bar, 100$\mu$m.
1275 (F) Thallus area of 15-day old gemmalings of WT, *Mpfer-1* mutant, and an amiR-
1276 Mp*FER*3-2 line growing on media containing different isoxaben concentrations (nM). n =
1277 30, outliers are indicated as black dots. Shown are means ± SEM of two biological
1278 replicates. Means designated by the same letter do not significantly differ at $P > 0.05$,
1279 one-way ANOVA, Duncan test.
1280 See also Figure S3
1281

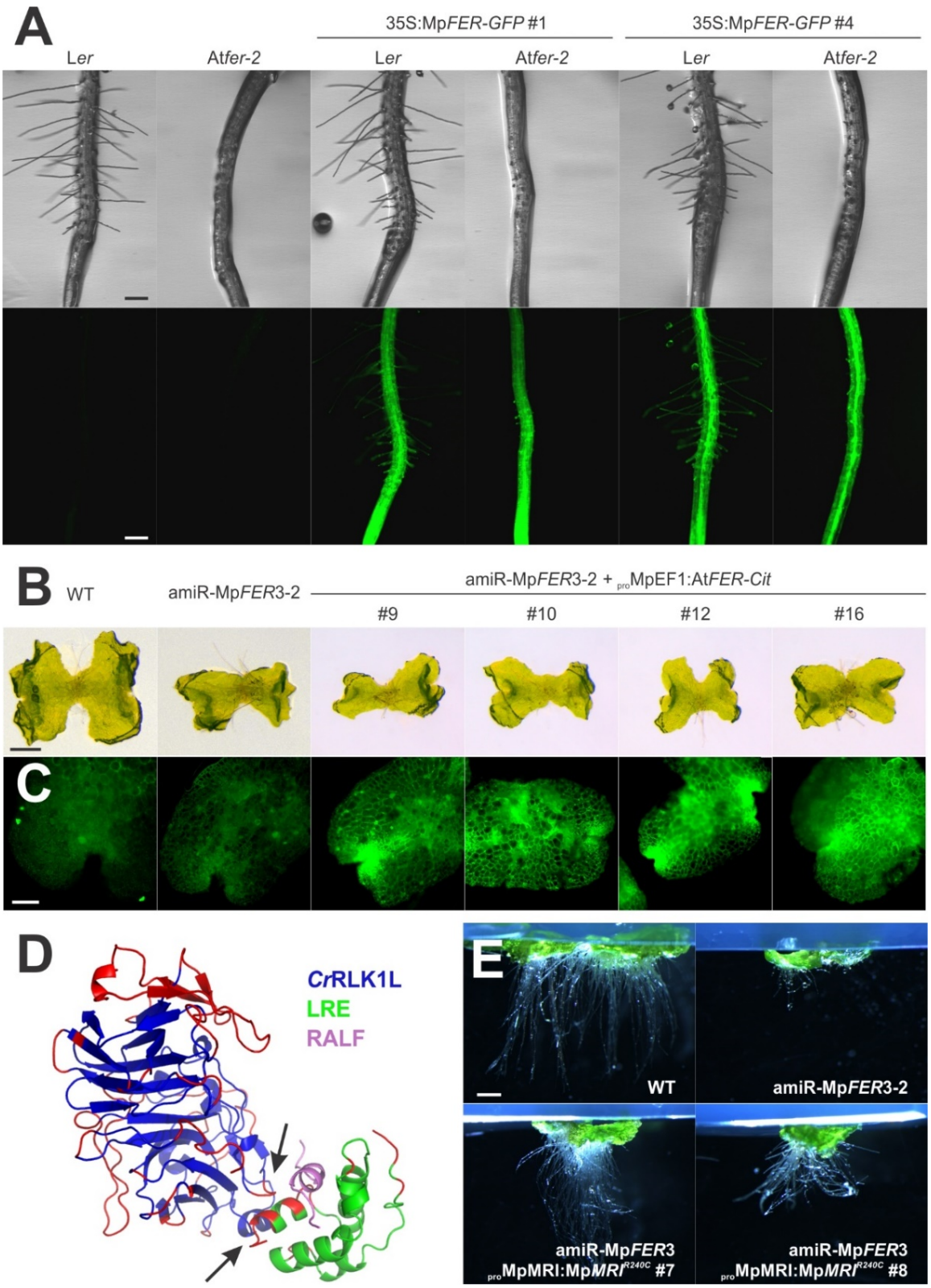


**Figure 6. Interspecific Complementation of *A. thaliana* and *M. polymorpha* Plants with Reduced Levels of *FER* Activity**

1286 (A) Roots of independent *A. thaliana* lines expressing 35S:Mp*FER-GFP* in L*er* wild-type
1287 (WT) and At*fer-2* plants. Scale bar, 200 µm.
1288 (B) 10-day old gemmalings of WT and amiR-Mp*FER*3-2 *M. polymorpha* plants with and
1289 without expression of At*FER-Cit*. Scale bar, 0.5 mm.
1290 (C) Citrine expression in 7-day old gemmalings of WT and amiR-Mp*FER*3-2 plants with
1291 and without expression of At*FER-Cit*. Scale bar, 100 µm.
1292 (D) Cartoon representation of the structural conservation of the *Cr*RLK1L$^{ECD}$/LRE/RALF
1293 complex by comparing AtFER/MpFER and AtLLG2/MpLRE1. Blue and green represent
1294 spatially highly conserved regions of *Cr*RLK1L and LRE homologs, respectively. Red
1295 indicates structural regions with low spatial conservation, lilac the C-terminal part of
1296 AtRALF23, and black arrows the interaction regions of the three proteins.
1297 (E) Complementation of amiR-Mp*FER* lines with a dominant-active version of Mp*MRI*
1298 under its own promoter ($_{pro}$Mp*MRI*:*MRI*$^{R240C}$). Scale bar, 1 mm.
1299 See also Figures S4-S7
1300

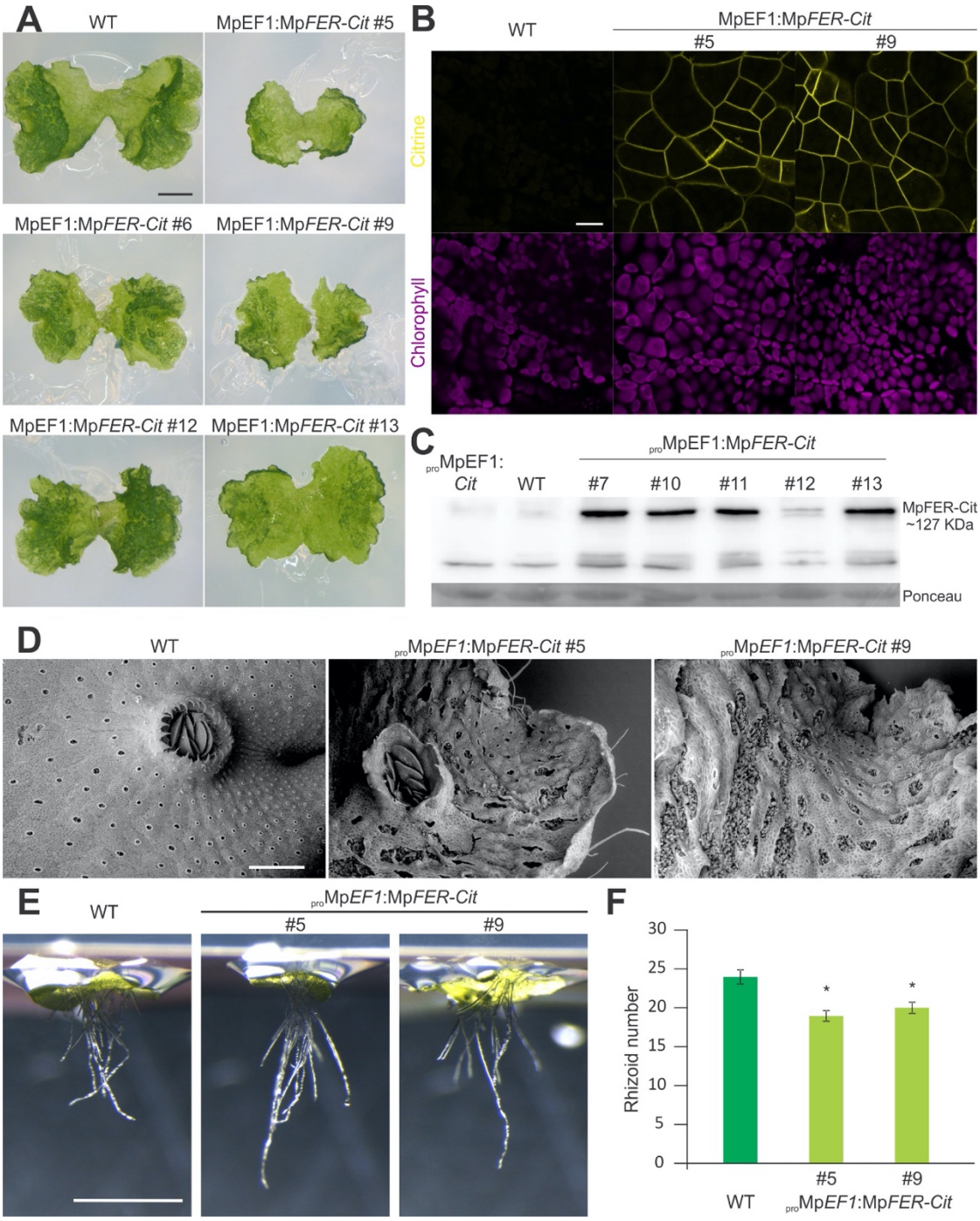


1301

1302

1303 **Figure 7: Overexpression of Mp*FER* Affects Morphological Integrity**

1304 (A) Representative pictures of 10-day old gemmalings of wild-type (WT, Tak1) and

1305 different lines overexpressing Mp*FER* ($_{pro}$Mp*EF1:*Mp*FER-Cit)*. Scale bar, 1 mm.

1306 (B) Citrine expression at the plasma membrane in WT and $_{pro}$Mp*EF1:*Mp*FER-Cit* lines #*5*
1307 and #9 as observed under confocal microscopy. Scale bar, 20 µm.
1308 (C) Western blot analysis of $_{pro}$Mp*EF1:*Mp*FER-Cit* lines using an anti-GFP antibody.
1309 $_{pro}$Mp*EF1:Cit* and WT lines were used as positive and negative controls, respectively. The
1310 Ponceau membrane staining of the most intense band at 55 kDa (presumably Rubisco)
1311 was used as a loading control.
1312 (D) Scanning electron microscopical images of thalli from 20-day old plants of WT and
1313 $_{pro}$Mp*EF1:*Mp*FER-Cit* lines #*5* and #9. Scale bar, 500 µm.
1314 (E) Representative pictures of 3-day old gemmalings growing in upside-down plates of
1315 WT and $_{pro}$Mp*EF1:*Mp*FER-Cit* lines #*5* and #9. Scale bar, 1 mm.
1316 (F) Number of rhizoids in 3-day old gemmalings of WT and $_{pro}$Mp*EF1:*Mp*FER-Cit* lines #*5*
1317 and #9. n = 30.
1318 See also Figure S6
1319

**A**

| | MpFER | | |
|---|---|---|---|
| **% Identity** | Malectin | ECD | Full protein |
| AtFER | 33.5 | 31.0 | 43.3 |
| AtANX1 | 29.8 | 26.5 | 39.8 |
| AtANX2 | 30.6 | 27.2 | 40.3 |
| AtTHE1 | 29.2 | 28.4 | 46.0 |

**B**

| % Identity | ECD CpRLK1 | CpRLK1 |
|---|---|---|
| MpFER | 25,7 | 29,2 |
| Mp1g17720 | 35,3 | 45,7 |
| AtFER | 28,0 | 41,5 |

**D**

| Qmean | $AtFER^{ECD}$ |
|---|---|
| MpFER | -3.79 |
| CpRLK1 | -5.05 |

**E**

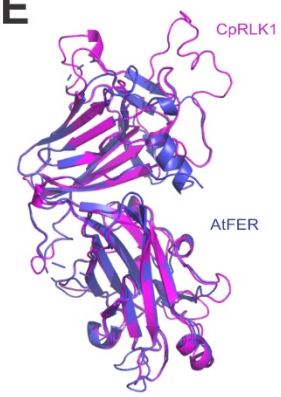


**C**

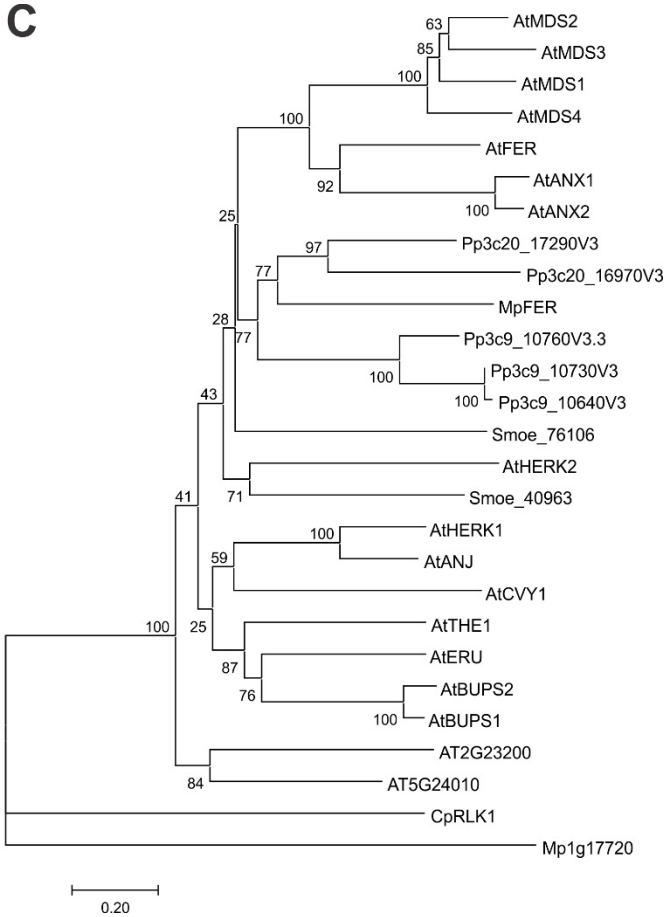


**Figure S1. The *Cr*RLK1L Family Appeared together with Land Plants. Related to Figure 1.**

(A) Percentage of identity of the malectin-like domain, the complete ECD, and the full protein of MpFER with AtFER, AtANX1, AtANX2, and AtTHE1.

(B) Percentage of identity of the ECD and full protein of CpRLK1 with MpFER, AtFER, and Mapoly001s0111.

(C) A rooted neighbor-joining tree of the amino acid sequence of the predicted malectin-like domain was generated using ClustalW. *Cr*RLK1L members from *Marchantia polymorpha* (Mp), *Physcomitrella patens* (Pp), *Selaginella moellendorffii* (Smoe), and *Arabidopsis thaliana* (At) were used. Algal CpRLK1 and Mapoly001s0111 were also included. The numbers indicate the bootstrap values (%) from 1000 replications. The given scale represents a substitution frequency of 0.1 amino acids per site.

1333 (D) Qmean value for prediction of MpFER or CpRLK1 3D structures of the ECD based
1334 on the AtFER ECD. Green numbers indicate a good modelling fit, red numbers indicates
1335 a bad modelling fit.
1336 (E) Structural superposition of the ECD of AtFER (blue) and CpRLK1 (purple).
1337

**A** Mp*miR160* Mp1g26670

GCACCTCCTCTCTCCGACTGCAGCCCGTTTCGAGATCCGAGGACTTGCTCGACGCGACTAATTGGGGAGGCCAGACTG
CACTTGCCTGGCTCCCTGTATGCCAACTGAGGAGCTCCTCAGAGACCTTGACAGGCTCCGTAGCTGGCATTCAGGGGG
CCATGCAGGAGGAAGTCGCTACCTCCCGCAAGGTGCGACTAGCTTTCTGTCTTGGGTGCACACCTCACTGATGTTTGA
TAGATTTACTTA

amiR-Mp*FER*1

**TGCAAGCTT**GCACCTCCTCTCTCCGACTGCAGCCCGTTTCGAGATCCGAGGACTTGCTCGACGCGACTAATTGGGGAG
GCCAGACTGCACTTGACGTAGGCAAACTTGTCGAACTGAGGAGCTCCTCAGAGACCTTGACAGGCTCCGTAGCTCGAC
ATGTTTGTCTACCTCAGGAGGAAGTCGCTACCTCCCGCAAGGTGCGACTAGCTTTCTGTCTTGGGTGCACACCTCACT
GATGTTTGATAGATTTACTTA**GGATCCATA**

amiR-Mp*FER*2

**TGCAAGCTT**GCACCTCCTCTCTCCGACTGCAGCCCGTTTCGAGATCCGAGGACTTGCTCGACGCGACTAATTGGGGAG
GCCAGACTGCACTTCGATGTCGAAAATCCAGGTGACTGAGGAGCTCCTCAGAGACCTTGACAGGCTCCGTAGCCACCT
GCATTTTTGACAACGAGGAGGAAGTCGCTACCTCCCGCAAGGTGCGACTAGCTTTCTGTCTTGGGTGCACACCTCACT
GATGTTTGATAGATTTACTTA**GGATCCATA**

amiR-Mp*FER*3

**TGCAAGCTT**GCACCTCCTCTCTCCGACTGCAGCCCGTTTCGAGATCCGAGGACTTGCTCGACGCGACTAATTGGGGAG
GCCAGACTGCACTTCCGAACTTCCTCAGAGACTCACTGAGGAGCTCCTCAGAGACCTTGACAGGCTCCGTAGCGAGTC
TGTGAGGGAGTTGGGAGGAGGAAGTCGCTACCTCCCGCAAGGTGCGACTAGCTTTCTGTCTTGGGTGCACACCTCACT
GATGTTTGATAGATTTACTTA**GGATCCATA**

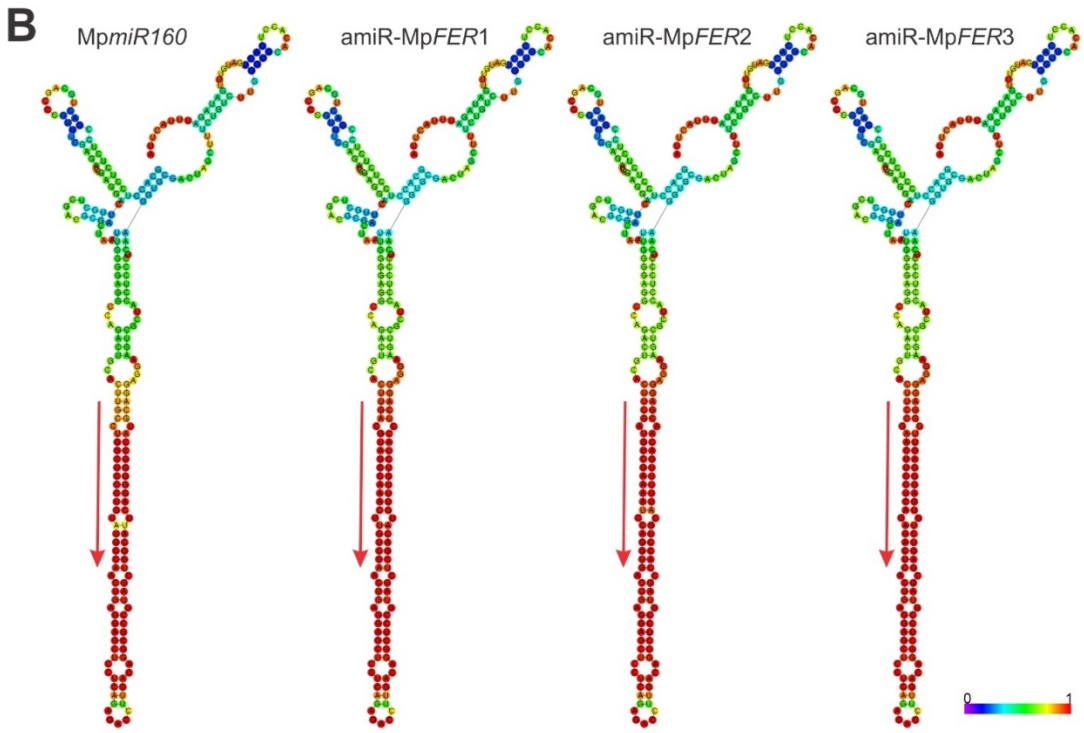


**Figure S2. Design of amiR-Mp*FER* Precursors. Related to Figure 3.**

(A) Mp*miR160* (Mapoly0002s0211, Mp1g26670) and amiR-Mp*FER*1, amiR-Mp*FER*2, and amiR-Mp*FER* sequences. miRNA sequences are in red and miRNA* in blue. Cloning sequences from amiR-Mp*FER* constructs are in bold.

1344 (B) Drawing of the minimum free energy structure of Mp*miR160* and amiR-Mp*FER*3
1345 constructs predicted by the RNAfold web server (http://rna.tbi.univie.ac.at//cgi-
1346 bin/RNAWebSuite/RNAfold.cgi). Red arrows indicate location and orientation of the
1347 mature miRNA in the precursor. The structures are colored by base-pairing probabilities;
1348 for unpaired regions the color denotes the probability of being unpaired.
1349

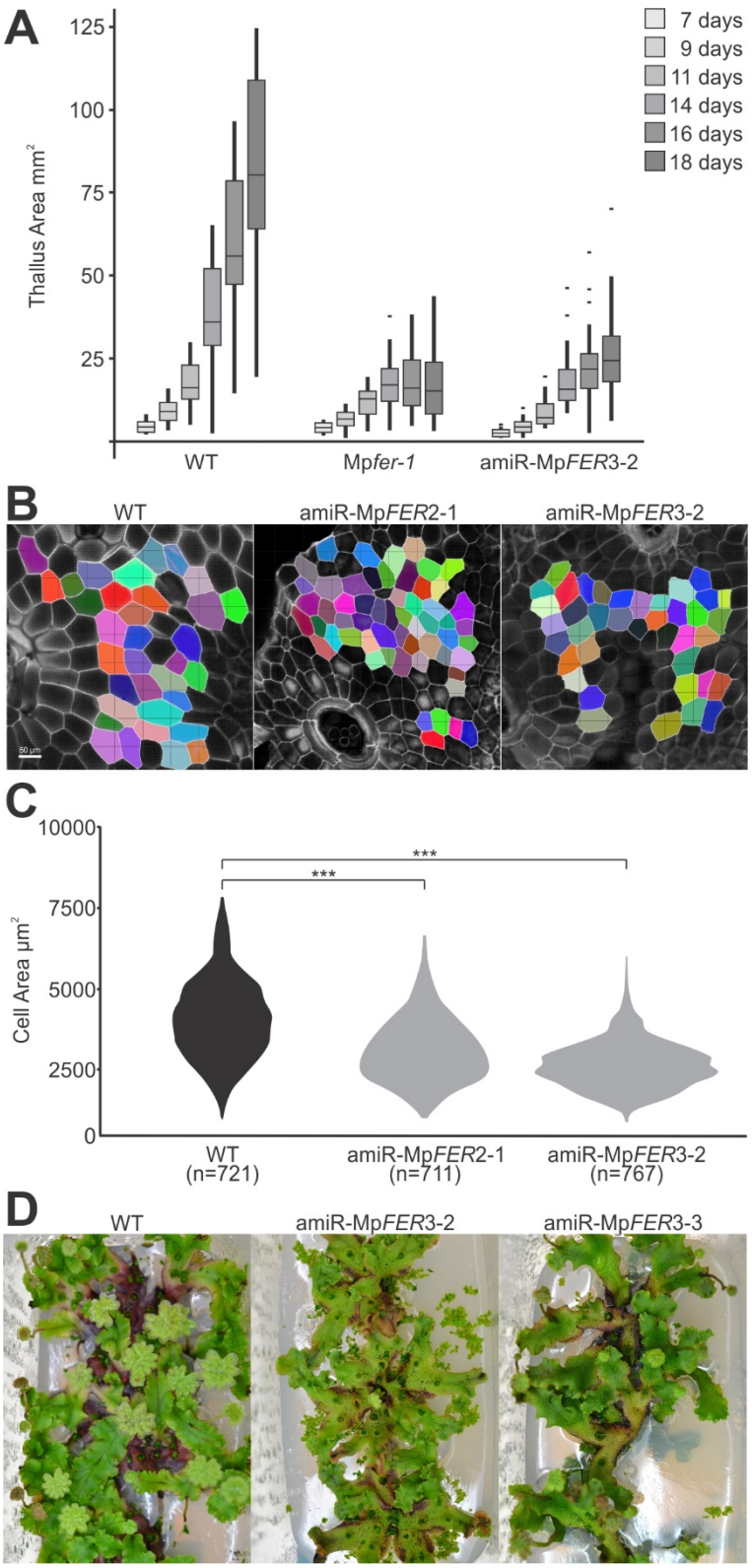


**Figure S3. Reduction in Thallus and Cell Area in Plants with Reduced Mp*FER* Levels. Related to Figures 3 and 5.**

1354 (A) Thallus area of wild-type (WT), Mp*fer-1*, and amiR-Mp*FER*3-2 plants at different days
1355 after putting gemmae on plates. n = 30, outliers are indicated as black dots. Areas were
1356 estimated using ImageJ software.
1357 (B) Representative images from cell surface areas measured in WT, amiR-Mp*FER*2-1,
1358 and amiR-Mp*FER*3-2 plants. Scale bar, 50 *μ*m.
1359 (C) Difference in cell size between WT, amiR-Mp*FER*2-1, *and* amiR-Mp*FER*3-2 plants is
1360 significant ($p<0.001$) based on the nonparametric Kruskal-Wallis test and a linear
1361 regression model with a highly significant interaction ($p<0.001$).
1362 (D) Induction of antheridiophores in WT and two independent amiR-Mp*FER*3 lines. Three
1363 plants were grown in each sterile plastic box under far-red light induction.
1364

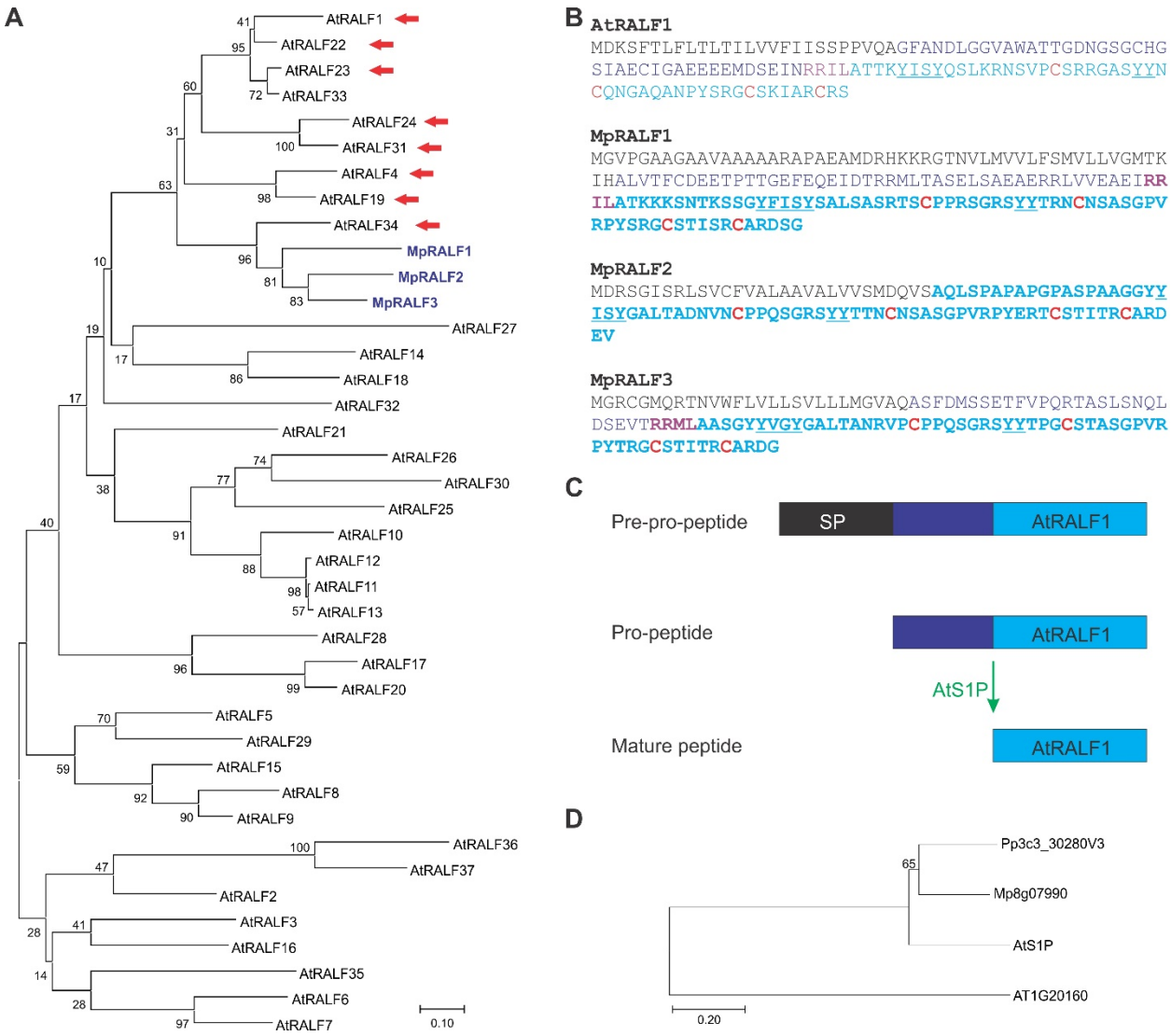


**Figure S4. MpRALF Peptides Belong to the AtRALF1-clade of the RALF Family. Related to Figure 6.**

(A) A rooted neighbor-joining tree of the amino acid sequence of the predicted mature RALF peptides was generated using ClustalW. RALF members from *M. polymorpha* and *A. thaliana* were used. Red arrows indicate RALFs that are known ligands of *Cr*RLK1Ls. The numbers indicate the bootstrap values (%) from 1000 replications. The given scale represents a substitution frequency of 0.1 amino acids per site.

1374 (B) Amino acid sequence comparison of AtRALF1 and MpRALF1-3. Predicted signal
1375 peptides are in black, predicted mature peptides in light blue, conserved Cys in red, and
1376 predicted S1P recognition sites in violet.
1377 (C) Processing pathway AtRALF1 by the S1P protease.
1378 (D) A rooted neighbor-joining tree of the amino acid sequence of the S1P orthologs was
1379 generated using ClustalW. S1P members from *M. polymorpha*, *P. patens*, and *A. thaliana*
1380 were used. The numbers indicate the bootstrap values (%) from 1000 replications. The
1381 given scale represents a substitution frequency of 0.1 amino acids per site.
1382

1383

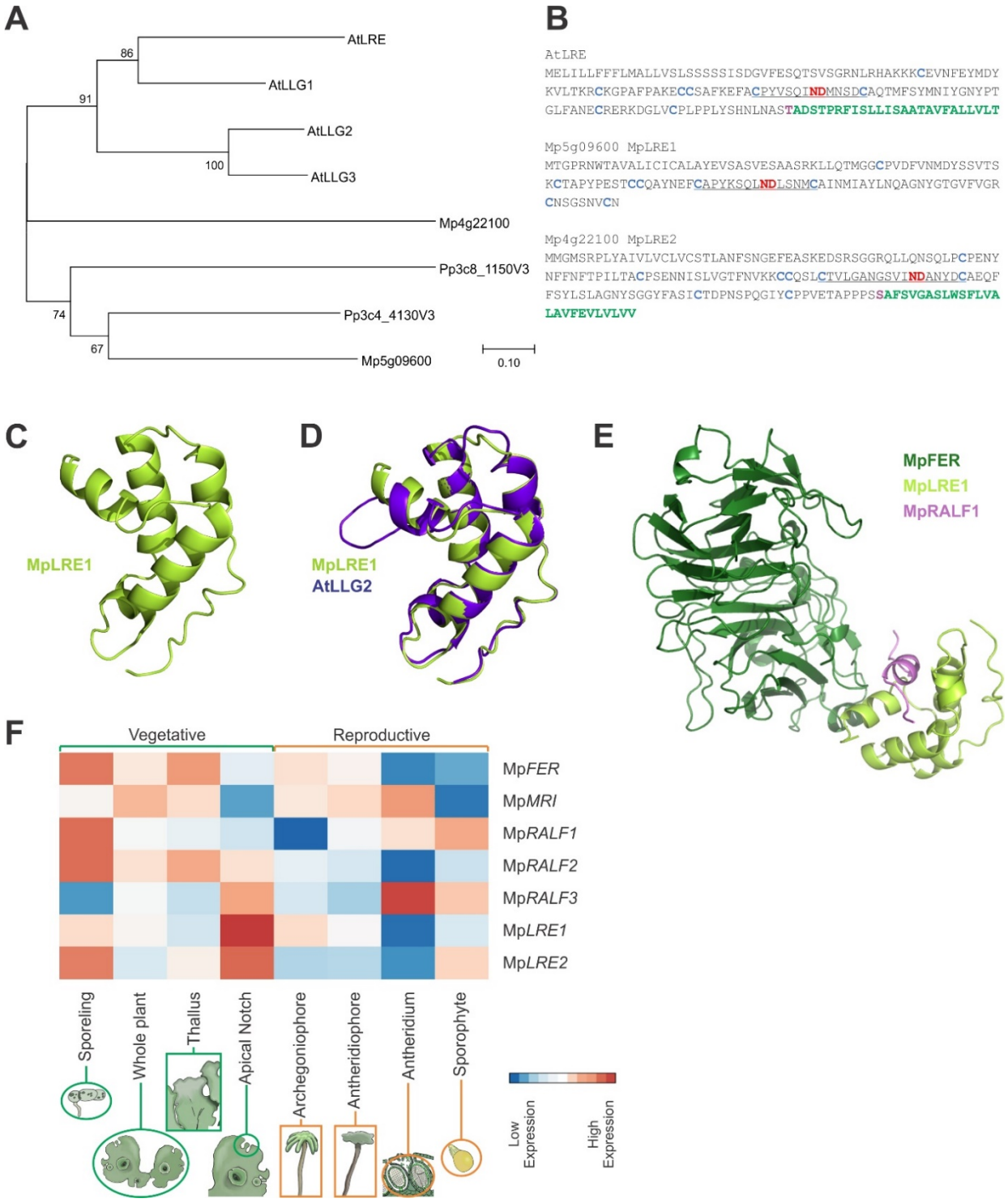


1384

1385

1386 **Figure S5. Two LORELEI-like Proteins Are Encoded in the *M. polymorpha* Genome.**

1387 **Related to Figure 6.**

1388 (A) A rooted neighbor-joining tree of the amino acid sequence of LRE orthologs was
1389 generated using ClustalW. LRE members from *M. polymorpha*, *P. patens*, and *A. thaliana*
1390 were used. The numbers indicate the bootstrap values (%) from 1000 replications. The
1391 given scale represents a substitution frequency of 0.1 amino acids per site.
1392 (B) Amino acid sequence of AtLRE, MpLRE1, and MpLRE2. Conserved Cys are in light
1393 blue, the ND motif in red, and the GPI-anchoring site in green.
1394 (C) Cartoon representation of the predicted 3-dimensional structure of MpLRE1, showing
1395 predicted alpha-helices.
1396 (D) Structural superposition of AtLGG2 (blue) and MpLRE1 (green).
1397 (E) Cartoon representation of the predicted 3-dimensional structure of the
1398 MpFER/MpLRE1/MpRALF1 complex, showing predicted alpha-helices and beta-sheets.
1399 (F) Heatmap depicting relative gene expression based on RNAseq data (row-Z-score of
1400 vs normalized counts) of Mp*FER* and the *M. polymorpha* orthologs of At*MR*l, At*RALF1*,
1401 and At*LRE* across different tissues. Vegetative and reproductive tissues are grouped by
1402 green and orange, respectively. Averaged expression values are represented with colors
1403 of increasing red and blue intensity indicating upregulation and downregulation of gene
1404 expression, respectively.
1405

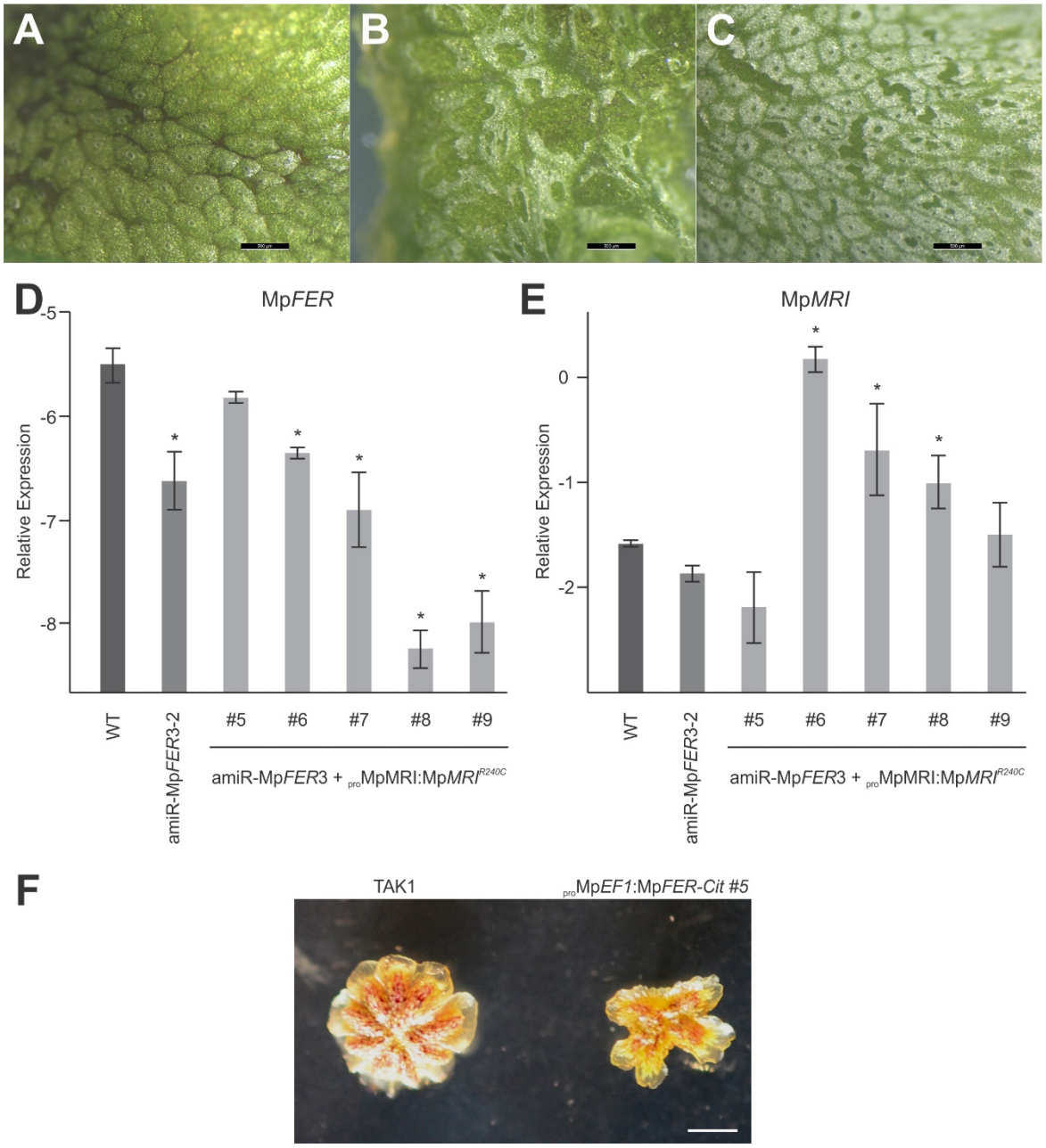


**Figure S6. Expression of Mp*MRI*$^{R240C}$ Suppresses the Bursted Rhizoid Phenotype of amiR-Mp*FER*3 Lines but Leads to Aberrant Epidermis Development. Related to Figures 6 and 7.**

1411 (A to C) Epidemical pictures of thalli from the wild-type (WT, Tak-1) (A), and amiR-
1412 Mp*FER*3 + $_{pro}$MpMRI:Mp*MRI*$^{R240C}$ lines #6 (B) and #8 (C), which both partially suppressed
1413 the bursting rhizoid phenotype (Fig. 6).
1414 (D and E) Relative expression of Mp*FER* (D) and Mp*MRI* (E) against the geometric mean
1415 of the reference genes Mp*ACT1*, Mp*ACT7*, and Mp*APT3* in WT, amiR-Mp*FER*3-2, and 5
1416 lines (#5 to #9) co-transformed with the amiR-Mp*FER*3-2 and $_{pro}$MpMRI:Mp*MRI*$^{R240C}$
1417 constructs. Expression levels of three biological replicates were assessed by droplet
1418 digital PCR (ddPCR). The y-axis corresponds to the log2-ratio between the test and the
1419 geometric mean of the reference genes. Shown are means ± SEMs of three biological
1420 replicates. *P < 0.01, one-way ANOVA.
1421 (F) Representative images of the antheridial receptacle of WT and $_{pro}$Mp*EF1:*Mp*FER-Cit*
1422 plants. Scale bar, 2 mm.
1423

**Figure S7. Structure Assessment and Quality Estimations of the MpFER and MpLRE 3-dimensional Models. Related to Figure 6.**

QMEAN score barplot indicating quality estimates of the predicted models, across their aminoacidic sequence. Below the barplots, the corresponding secondary structures are displayed for both target and template sequences, with alpha-helixes represented by light purple boxes and beta-sheets by green arrows. All plots were adapted from the model report produced by the SWISS-MODEL workspace.

(A) MpFER$^{ECD}$, for which AtFER was used as a template (PDB 6a5b.1A).

(B) MpLRE1, for which AtLLG2 was used as a template (PDB 6a5d.1A).